

NASA-TM-107,763

**NASA Technical Memorandum 107762**

NASA-TM-107763 19940008331

**The MRIS Feasibility Study**

**Robert T. Neece, Aubrey E. Cross, and  
James H. Schrader**

**FOR REFERENCE**

**NOT TO BE TAKEN FROM THIS ROOM**

**June 1993**

**NASA**

National Aeronautics and  
Space Administration

**Langley Research Center**  
Hampton, Virginia 23681-0001

**LIBRARY COPY**

SEP 17 1993

**LANGLEY RESEARCH CENTER  
LIBRARY NASA  
HAMPTON, VIRGINIA**



## Preface

The objective of the Microwave Reflectometer Ionization Sensor (MRIS) Feasibility Study was to develop and demonstrate an experimental millimeter wave system that could make distance measurements of the type that an MRIS flight instrument would be required to make. This experimental system was to provide sufficient confidence that the technical problems were surmountable within the constraints of the Aeroassist Flight Experiment schedule and budget. Subsequently, the experience provided by the MRIS Feasibility Study was applied to the development of the instrument requirements, and the first manuscript of this document was included with the Request for Proposals issued to initiate the contracted effort for the flight instrument development. That manuscript has been edited and is now being formally published as a part of the documentation recording the MRIS experiment, especially to provide background for subsequent documents.

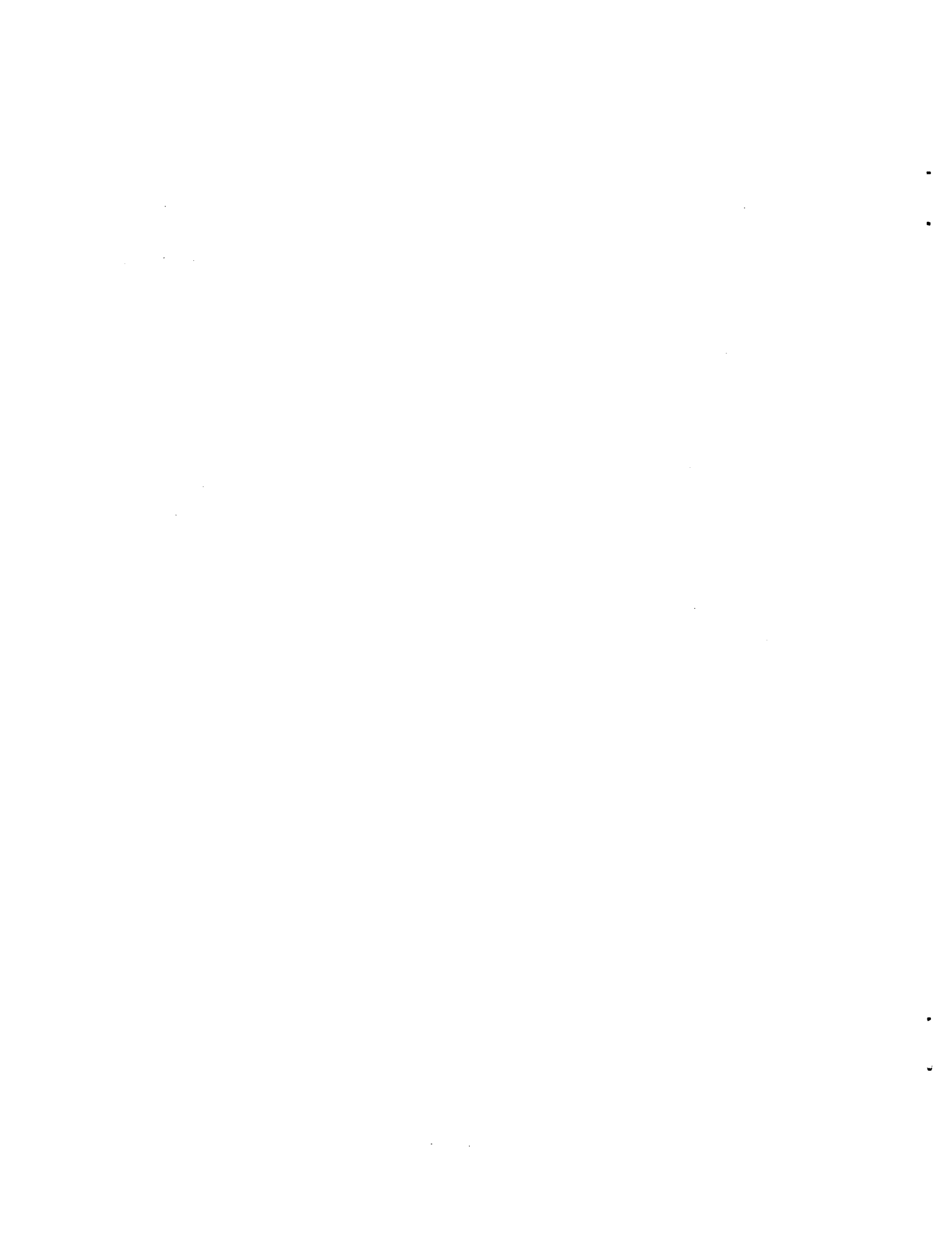
The work reported here was carried out from 1987 to 1989, and the results and conclusions herein represent the thinking at that time. The study was carried out primarily as a hardware experiment with little theoretical underpinning. Following the Feasibility Study, the instrument development program was contracted, and parallel in-house studies were pursued. At the time of this writing (1993), there is considerably more knowledge of, and appreciation for, the impact of parallel-plate propagation effects on active distance measurements involving measurement of the reflection coefficient as a function of frequency. The interpretations of the early experimental work, reported here, lumped those effects with multiple reflection effects.

The design approach developed by the instrument contractor, Electromagnetic Sciences, Inc., departed from the experimental system described here and applied the techniques used in vector network analyzers. The distance measurements relied on the measurement of reflection coefficient as a function of frequency and the conversion of these data to the time domain. The deleterious effects of parallel-plate propagation became a serious concern, and subsequent MRIS laboratory efforts focused largely on understanding these problems.

The design and development of the experimental model and the hands-on conduction of the work described here was carried out by my coauthors, Jim Schrader and Aubrey Cross. Both retired, they deserve the appreciation of all the MRIS team for providing the foundation for our work. Aubrey Cross continued as a part of the team, throughout the life of the project, and provided an invaluable resource in all our laboratory investigations.

## Abstract

The Microwave Reflectometer Ionization Sensor (MRIS) is an instrument being developed for use in detection and ranging of electron density layers in the reentry plasma of a space transfer vehicle. This paper presents the rationale for the selection of the double sideband suppressed carrier (DSBSC) system used in the Feasibility Study for the MRIS. A 25 GHz single-oscillator system and a 220 GHz double-oscillator system are described. The 25 GHz system was constructed and tested in the laboratory and test results are presented. As developed, the system employs a sideband spacing of 160 MHz. Based on an estimated electromagnetic wave velocity in the plasma, a round-trip phase shift measurement accuracy of  $\pm 7.6^\circ$  was required for the desired  $\pm 1/2$  cm distance measurement accuracy. The interaction of parallel ground and reflecting planes produces interference that prevents the basic DSBSC system from meeting the accuracy goal, so a frequency modulation was added to the system to allow averaging of the measured phase deviation. With an FM deviation of  $\pm 1$  GHz, laboratory measurements were made for distances from 5 to 61 cm in free space. Accounting for the plasma velocity factor, 82 percent of the data were equal to or better than the desired accuracy. Based on this measured result, a sideband spacing to 250 MHz could be expected to yield data approximately 96 percent within the accuracy goal.



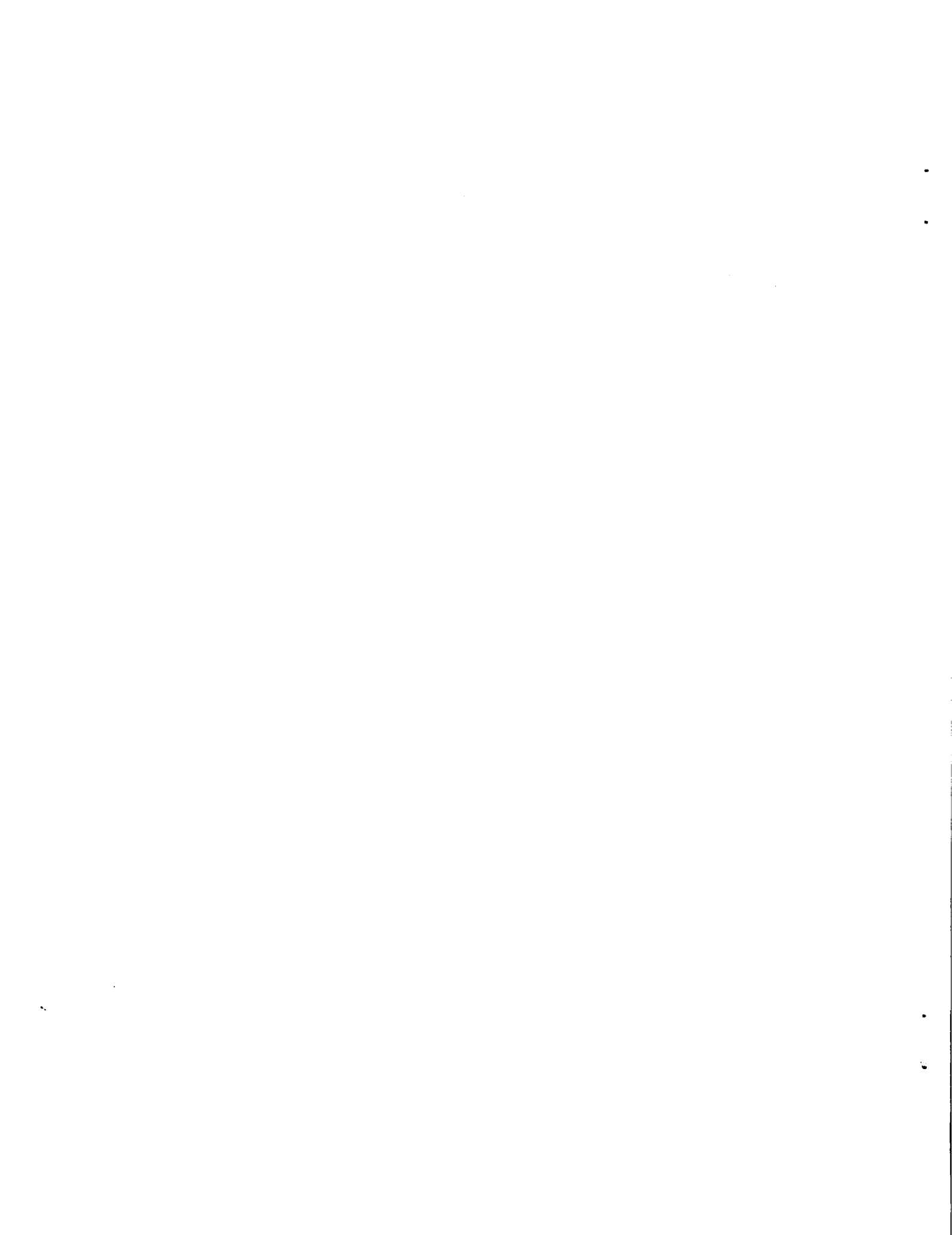
## Contents

Preface	i
Abstract	iii
Symbols and Abbreviations	vi
1.0 Introduction	1
1.1 MRIS Objectives	1
1.2 Feasibility Study Objectives	3
2.0 Plasma Effects and Data Reduction Studies	5
2.1 Electromagnetic Wave - Plasma Interactions	5
2.2 Plane Wave Propagation	7
2.3 Antenna Effects in the Presence of Plasma	9
2.4 Dynamic Signal Effects	10
3.0 Measurement Techniques	12
3.1 Frequency Measurement	12
3.2 Phase Measurement	13
4.0 Dual Frequency Instrument Configurations	15
4.1 Single Oscillator System	15
4.2 Two Oscillator System	16
5.0 Single Oscillator, 25 GHz System Development	17
5.1 Initial Development and Evaluation	17
5.1.1 Direct Transmission and Evaluation	19
5.1.2 Reflected Path Tests With No Ground Plane	19
5.1.3 Reflected Path Tests With a Ground Plane	20
5.2 Modification and Evaluation With Frequency Modulation	22
5.2.1 FM Implementation and Tests	22
5.3 Analytic Model Comparison	24
5.3.1 Model Description	24
5.3.2 Comparison of Model and Experimental Data	25
5.4 Discussion of Results to Date	25
6.0 Conclusions	28
7.0 Continuing Efforts	29
List of References	30

## Symbols and Abbreviations

AFE	Aeroassist Flight Experiment
AGC	automatic gain control
AM	amplitude modulation
c	speed of light
CFD	computational fluid dynamics
d	electron density
D	distance to the reflecting plane
$\delta F$	change in frequency
$D_r$	minimum resolvable distance
DSBSC	double sideband suppressed carrier
$D_u$	unambiguous range of detection
$\epsilon$	effective dielectric constant
$\epsilon_0$	permittivity of free space
f	electrical frequency
$f_c$	collision frequency
$F_d$	difference frequency
FM	frequency modulation
FM-CW	frequency-modulated continuous wave
FM LIN	FM linearity
$f_p$	plasma frequency
$F_r$	minimum resolvable frequency
$\eta$	index of refraction
IF	intermediate frequency
m	electronic mass
MRIS	Microwave Reflectometer Ionization Sensor
$N_{ECR}$	critical electron density
$\theta$	phase angle
q	electronic charge
REC NOISE	receiver noise
RF	radio frequency
SNR	signal to noise ratio
STV	space transfer vehicle
$T_m$	measurement period
TPS	thermal protection system

UHF	ultra high frequency
$v_g$	group velocity
$v_p$	phase velocity
XMIT PWR	transmitter power



## **1.0 Introduction**

The Microwave Reflectometer Ionization Sensor (MRIS) is being developed in conjunction with the Aeroassist Flight Experiment (AFE), an experiment intended to investigate a new flight regime which will be encountered by aerobraking spacecraft. The impetus for this study is the need for a Space Transfer Vehicle (STV) that will be used to transfer payloads from high Earth orbit to low Earth orbit by passing through the upper atmosphere for braking, rather than relying on retrorockets. These vehicles will be characterized by large blunt heat shields which serve as aerobrakes. The shock layer formed in front of the heat shield during the aerobraking maneuver will exhibit properties unlike those encountered before.

The AFE will return flight data necessary for the design of future STV's. The flight experiment will provide significant results in many STV technology areas, such as definition of radiative and convective heating levels, aerodynamic performance and flight control, and thermal protection system (TPS) performance. The data will also be used to develop and verify prediction methods and flow field computation techniques for this flight regime.

The MRIS instrument is envisioned as a multiple frequency device mounted under the TPS tiles for measurement of electron densities in a non-intrusive manner using millimeter wavelengths. A feasibility study has been conducted in order to outline the appropriate characteristics that the instrument should have and to identify methods for accomplishing the measurement task. This document is a summary of the findings of that study through October 1988.

### **1.1 MRIS Objectives**

The MRIS is intended to use the reflective properties of the high temperature plasma to determine levels of electron density in the shock layer and to determine their distance from the aerobrake surface. Figure 1 shows the aerobrake and the shock layer and illustrates the role of MRIS. Information about the electron density profile versus distance from the aerobrake surface will be useful in the study of wall catalysis (the catalytic effect of the TPS surface on the plasma), radiative heating, and flow field dynamics.

The achievement of the MRIS objectives will be dependent upon the sensor itself and upon the complementary analysis, because the sensor will not make a direct measurement of distance. The MRIS instrument will be required to measure the presence of specific electron densities in the range from  $10^{12}$  to  $10^{15}$  electrons per  $\text{cm}^3$  and to measure the signal propagation time to each density from the surface of the aerobrake, at distances within the range from 0 to 30 cm. Subsequent to the measurements, analysis will be used to estimate distance based on signal propagation time.

The distance to the critical electron density is referred to as the standoff distance. Electromagnetic waves of a particular frequency,  $f_p$ , will be reflected when the electron density in the plasma reaches the critical electron density,  $N_{\text{ECR}}$ , as defined by the equation

$$N_{\text{ECR}} = 1.24 \cdot 10^{-8} \cdot f_p^2 \quad (1)$$

where  $f$  is given in Hz and  $N_{\text{ECR}}$  is in electrons per  $\text{cm}^3$ .

Specifically the five MRIS experiment objectives are:

- 1) Measure the power of the plasma-reflected signals from several microwave signal generators (at selected frequencies) to detect the onset, presence, and decay of the critical electron density corresponding to each frequency as a function of AFE vehicle flight time.
- 2) Compare the detected electron density information, using flight conditions for the AFE vehicle (altitude, velocity, etc.), with predictions using flow field calculations, which include finite-rate chemical and ionization reactions, to confirm the accuracy of the calculation method and reaction model used.
- 3) Measure the propagation times of the signals reflected from the ionized flow field as a function of AFE vehicle flight time. Estimate the standoff distances to the location of the critical electron densities detected using

the experimentally measured propagation times along with analytically derived propagation characteristics.

- 4) Compare the calculated standoff distance information, using flight conditions for the AFE, with the predicted standoff distance data from the computational fluid dynamics models for the AFE trajectory.
- 5) Measure the reflection coefficient at the input of each transmitting antenna to determine if the critical electron density has been reached at the antenna covering (TPS tile) surface. Determine times of on-set and decay of these critical electron densities.

## 1.2 Feasibility Study Objectives

The methods employed to determine the feasibility of the MRIS have involved two parallel efforts: problem analysis and instrument development. The analytic effort has explored the characteristics of wave propagation in the plasma and the ability to model that propagation for purposes of developing the instrument and reducing the data returned from the instrument. The development effort has been directed at demonstrating the ability to make the required measurements with the required accuracy (or showing that the required accuracy could be achieved). Both efforts rely in part on present abilities to predict the composition and profile of the plasma shock layer.

The objectives of the development effort were as follows:

- Develop and experimentally evaluate two sensor designs which operate at frequencies corresponding to critical electron densities at the high and low end of the required range.
- Simulate standoff distance measurements by making measurements to a reflecting metal plate.
- Measure reflected power over a dynamic range sufficient to reliably detect the presence of the reflecting surface out to 30 cm standoff distance (based on the propagation and reflection characteristics estimated for the plasma).

- Measure distance unambiguously to an accuracy corresponding to  $\pm 1$  cm or better out to 30 cm standoff distance (based on the expected propagation and reflection characteristics of the plasma).
- Evaluate the TPS tiles as coverings for the antennas, and determine the effects of the TPS system on the instrument operation.
- Evaluate models for the plasma sheath ahead of the vehicle, and assess the effects of the plasma properties on the measurement process.
- Develop vigorous full-wave solutions to characterize the performance of aperture antennas located on a ground plane under TPS tile coverings and in the presence of an inhomogeneous plasma sheath.

The experimental evaluations of instrument design have been obtained with measurements of the standoff distance to a metal plate acting as a crude simulation of a critically dense plasma. The instrument design, however, must function in the presence of an actual plasma. A discussion of plasma effects will be given here first to establish the background for the remainder of the document.

## **2.0 Plasma Effects and Data Reduction Studies**

Analytical studies have been performed to establish a model for the interaction of the electromagnetic fields excited by the aperture antennas and the plasma sheath surrounding the vehicle. The studies have sought to define those features of this interaction that impact the design of the MRIS instrument and the reduction of data to be obtained in the experiment. Results of the studies include an assessment of those plasma effects that are likely to affect the measurements as well as full-wave solutions for the coupling between the source and receiving apertures in the presence of layered dielectrics (e.g., tiles and bond layers), reflecting metal plates, and plasma media. In addition, use has been made of the best estimates for electron density profile shapes and amplitudes that are available from the computational fluid dynamics community at this time.

It is not the intention to cover here all aspects of the ongoing studies of plane wave propagation within the plasma or the investigation of means for the reduction of the data. Instead, the information given is to provide some background on expected plasma effects so that a potential instrument development contractor could weigh these effects on his instrument design.

### **2.1 Electromagnetic Wave -- Plasma Interactions**

Plasma interaction with electromagnetic fields results in a number of resonant phenomena. Fortunately, most of these resonances occur at frequencies much below the millimeter wave driving frequencies under consideration here. Of those phenomena associated with a dominant magnetic field (the Earth's field in this case), the highest cyclotron frequency (that of the electrons) lies well below the lowest frequency of interest to the MRIS, and the radii of gyration of the charged particles are much larger than the electromagnetic wavelengths (Ref. 1). Thus, only "ordinary mode" propagation needs to be considered.

For the case at hand, there are three principal parameters of the plasma that characterize the interaction problem. The first is the plasma frequency,  $f_p$ , whose square is given by the expression

$$f_p^2 = (1/4\pi^2) q^2 d / \epsilon_0 m \quad (2)$$

where  $d$  is the electron density,  $q$  is the charge on the electron,  $\epsilon_0$  is the permittivity of free space, and  $m$  is the electronic mass (MKS units are used). The plasma frequency is the natural frequency (measured in Hertz) of oscillation of the electrons when their charge center is displaced from that of the background ion population. Its magnitude is determined by the interplay of the Coulomb force and the electron inertia.

The second parameter is the frequency of collisions between the electrons and the background ions and neutral particles. These collisions are responsible for the dissipation of electromagnetic energy and introduce losses into the propagation path. The collision frequency depends on the electron number density and the kinetic temperature of the electrons.

The third parameter is the Debye length, which can be regarded as the distance that an electron can travel during one period of the plasma frequency and is the distance over which the plasma can screen itself from applied electric fields. When the Debye length approaches the electromagnetic wavelength, it is possible for energy to be coupled into purely electrostatic plasma modes and with a non-zero electron temperature, for this coupled energy to be propagated away and subjected to a damping process known as collisional Landau damping. For the MRIS situation, the Debye length is so short that this process, if it occurs at all, can happen only very near the reflection point of the electromagnetic wave, and its results would be a very slight shift in the effective local plasma frequency and a slightly lowered reflection coefficient at that point.

For the MRIS, the interaction process can be regarded as the propagation of electromagnetic waves through a medium that is inductively loaded because of the electron inertia (plasma frequency effects) and that is subject to a loss

mechanism due to collisions. If collisions were negligible, this situation would result in an effective dielectric constant  $\epsilon$  given by

$$\epsilon = 1 - f_p^2 / f^2 \quad (3)$$

At a point where the electron density (and hence  $f_p$ ) becomes large enough to make  $\epsilon$  negative, the wave cannot propagate further and becomes evanescent (in analogy with fields in a waveguide beyond cut-off), and the energy in the wave is turned back.

Collision effects are added to this description by introducing the collision frequency as an imaginary part,  $f_c$ , of the wave frequency  $f$ . The result is a complex dielectric constant given by

$$\epsilon = 1 - f_p^2 / (f^2 + f_c^2) - j f_c f_p^2 / (f(f^2 + f_c^2)) \quad (4)$$

For the MRIS, the collision frequency is expected to be much smaller than the wave frequency, so that the major results are a slight shift in the position of the turning point (due to the real part of epsilon) and the introduction of losses (due to the imaginary part). Typical values to be expected for  $f_c$  are about 200 MHz.

## 2.2 Plane Wave Propagation

A plane wave propagating in the plasma medium will have a phase velocity related to the index of refraction,  $\eta$ , which in turn is the square root of epsilon given above. Thus

$$\eta = \epsilon^{1/2} \quad (5)$$

and the phase velocity,  $v_p = c/\eta$ , where  $c$  is the free-space velocity of light. Since the velocity depends on the local electron density and the wave frequency, the medium is dispersive.

Consider a single-frequency wave propagating into an increasing electron density from some reference position. After reflection at its turning point, the wave returns to the reference point with a definite phase shift relative to the original wave. This phase shift is proportional to twice the integral over the one-way distance of the reciprocal of  $v_p$ . A known variation of  $\eta$  with distance (i.e., a known electron density profile) allows computation of this phase shift. Alternatively, it would be desirable to use a measurement of the phase shift to get information about the two-way distance or about the profile of  $\eta$ . Such an approach is ambiguous in two ways. First, if the distance to the turning point is larger than one-half wavelength, then the phase shift is larger than  $360^\circ$ , and the phase shift itself is ambiguous. Second, the upper limit of the above-described integral is the actual distance to the turning point and the integrand depends on the profile shape of  $\eta$ . Thus, an unambiguous inversion of the integral equation is not possible in the general case.

The ambiguities encountered in this integral inversion are (partially) resolvable by two means: use of a modulating envelope rather than a single carrier frequency and use of repeated measurements in several frequency bands. The use of a modulating envelope allows the unambiguous range of the measurement to be extended to one-half the wavelength of the modulation frequency. The use of repeated measurements in several frequency bands will provide data points for the calculation of the electron density profile based on the assumption of a lower bound for the electron density, a monotonically increasing density, and an assumed shape for the density function between data points. A third alternative, judged impractical for MRIS, consists of making closely spaced (or continuous) single carrier frequency measurements over all frequencies from a value low enough to have an unambiguous phase shift to a value high enough to probe into high density profile. An essential continuum of measurements of this kind would allow the above-described integral equation to be mathematically inverted to find the profile variation of the index of refraction  $\eta$ .

A modulation envelope propagates at the group velocity,  $v_g$ . If the desired phase shift affects the envelope rather than the carrier, then by analogy with the above discussion the phase shift is proportional to twice the integral over the one-way distance to the turning point of the reciprocal of  $v_g$ . With the

wavelength of the envelope being longer than twice the turning-point distance, the phase shift will be less than  $360^\circ$ , and the first ambiguity is resolved. Repeating this measurement over many separated frequency bands and making an assumption about the shape of the profile between the respective turning points for each frequency band (e.g., that it is linear between these points), allows one to find the distances to the turning points. This solution is analogous to the inversion of the integral equation mentioned above.

For the MRIS, the situation is somewhat more complicated than the simple plane wave model above would indicate. The waves must be launched and received by antennas for which the plasma lies in the near field and for which interfering or multiple reflections between the plasma, TPS, and antenna ground plane are important. Although simplified, multiple ray-tracing solutions have been found to be accurate for measurements against a calibrating flat metal plate as discussed in Section 5.0 below, it is expected that full wave solutions are necessary for the plasma case. Such solutions have been developed as part of the feasibility studies.

### 2.3 Antenna Effects in the Presence of Plasma

Up to the present, the radii of curvature of the AFE vehicle forebody surface and of the plasma sheath have been assumed large enough to be modeled by flat surfaces or planar layers. Antennas are then modeled as aperture antennas in a ground plane with appropriate covering by thermal protection system (TPS) tiles. Beyond the tiles, the plasma sheath is assumed to have density gradients normal to the antenna ground plane with no lateral variation. The electron density is taken to rise monotonically from the TPS surface, rapidly at first and then more gradually, reaching a peak 15 to 30 cm from the surface, and then falling abruptly to very low values. For design purposes, the peak electron density, under maximum conditions, may be about  $6 \times 10^{15}$  electrons per cubic centimeter.

The feasibility studies have included full wave solutions to both the single antenna and two-antenna geometries for circular apertures having both single and multimodal circular waveguide field distributions in the apertures.

The ultimate calculations are the self-admittance of the transmitting aperture and the mutual admittance of the receiving aperture in the presence of plasma and/or TPS tiles. From these values, the phase shifts between transmitted and received signals can be calculated for each constituent frequency of the measurement process. Preliminary calculations yield high confidence that the computational methods used are adequate for the plasma modeling that has been adopted. These methods will be used to compute the behavior of the MRIS instrument for various plasma profiles as an aid in the data reduction and to assess the effects of instrument parameters on the deduced standoff distances.

Since the apertures excite and respond to an entire angular spectrum of plane waves, with both parallel and perpendicularly polarized scattering from the plasma, the sizes of the aperture and the distribution of fields within them strongly affect the associated admittances and the instrument response to the plasma. For given size apertures, the mutual admittance in the absence of plasma varies in a somewhat oscillatory fashion with separation distance, so that an optimal spacing results for a given size. In turn, there are several factors involved in the selection of aperture size.

Large apertures have higher gain and (when properly spaced) have less undesired coupling than smaller ones. Also, they can give useful return power for large plasma standoff distances. For short standoff distances, however, the scattered signal from the medium tends to be smaller because of the reduced overlap of the patterns. Thus, a compromise must be reached to cover the entire range of desired standoff distances. These factors are thoroughly discussed in Section 5.0 in connection with the flat metal plate scattering experiments.

#### 2.4 Dynamic Signal Effects

The discussion to this point has centered on a plasma model with a static electron distribution and with no lateral density variations. Such a model is appropriate for a smooth, laminar, fluid flow near the stagnation point of the forebody, with changes in the electron density occurring on a slow time scale as the AFE changes altitude. While the effects cannot be quantified at this

point, there are possibilities for additional dynamic behavior which could substantially affect the MRIS measurement if they were present.

The first such effect could be an effective longitudinal oscillation of the apparent reflecting layer such that Doppler shifted reflections would occur, with differing values for different angles of incidence. Conventional Computational Fluid Dynamics (CFD) models do not allow for such oscillations, but shadowgraph images from ballistic test ranges suggest their plausibility. Such images taken for hypersonic blunt bodies often show striated variations in the density between the shock front and the body surface. One explanation for these striations is the reverberation of acoustic signals that could be induced by vibrations related to vortex shedding by the vehicle. If such density variations occur under the AFE flight conditions and if their origin has such a dynamic cause, they could well produce an unwanted Doppler spectrum on the reflected signals of the MRIS. Additionally, it is conceivable that small density fluctuations could exist in the transverse direction in the plasma sheath. If the scale size of these density variations were found to be comparable with the electromagnetic wavelength in the plasma, then off-normally incident waves would produce nonspecularly scattered components and these would be Doppler shifted.

It may be determined that the MRIS instrument must allow for the existence of such Doppler spectra as a contaminant on its primary data mission. The strength and spectral extent of these fluctuating Doppler signals is not known, however, they could easily reach a few tens of kilohertz. A possible solution might be to low-pass filter all primary data to ensure that stable, nonaligned results are obtained.

Although removal of these Doppler shifts is desirable for the standoff distance measurement, a qualitative measurement of their existence would be of much scientific value. Consideration has been given to the possibility of measuring the Doppler spectral power in a collection of narrow band-pass filters placed within a few kilohertz of the carrier frequencies and monitored at a low sampling rate.

### 3.0 Measurement Techniques

Several measurement techniques were considered before choosing the general approach to be taken for the feasibility study. These consisted of frequency and phase measurement schemes which are reviewed here. For purposes of comparison, these assumptions were made: a 24 GHz operating frequency; unambiguous distance measurements over a minimum range of 40 cm with an accuracy of  $\pm 1$  cm; and 10 data points per second. At the time of this preliminary evaluation little was known about the losses or velocity for propagation in the plasma, so free space parameters were used.

#### 3.1 Frequency Measurement

One of the first radar systems considered for this application was the frequency-modulated continuous wave (FM-CW) system (Ref. 2). The general form for an FM-CW system is illustrated in figure 2. When the transmit frequency is modulated periodically with time, the time delay associated with the round trip propagation causes the received signal to lag the transmitted signal in frequency. By mixing the two, the range to the reflection point can be inferred from the difference frequency which is a function of the propagation time delay. (For a moving target, Doppler also affects the difference frequency, but with the appropriate modulation Doppler can be processed out of the data.)

Consider a transmitting source with a constant rate-of-change of frequency over the measurement period,  $\delta F/T_m$ . For a stationary target, the difference frequency,  $F_d$ , equals the propagation delay times the rate of frequency change and is given by

$$F_d = 2 \cdot \delta F \cdot D / (c \cdot T_m) \quad (6)$$

where  $D$  is the distance to the reflecting plane and  $c$  is the speed of light. This equation is easily solved for the distance as a function of the difference frequency. For a system using cycle-counting for frequency measurement, the minimum resolvable frequency is  $1/T_m$ , so the minimum resolvable distance ( $D_r$ ) is linked to the measurement period. Substituting with the

minimum resolvable frequency,  $F_r = 1/T_m$ , and solving for the minimum resolvable distance gives

$$D_r = c/(2 \cdot \delta F). \quad (7)$$

In this case, the minimum resolvable distance should be  $\leq 1$  cm and the measurement period should be  $\leq 0.1$  sec., resulting in a required bandwidth of greater than 50 percent at a carrier frequency of 24 GHz.

The primary advantage of the frequency measurement technique is that it is possible to isolate and measure various reflecting points along the transmission path through spectrum analysis. The primary disadvantages are:

- 1) considerable sophistication in both the transmitter and receiver,
- 2) difficulty in obtaining the RF sources and antenna(s) with the required bandwidth,
- 3) high output data rate, and
- 4) interfering signals, within the spectrum of the desired received signal, at the mixer.

To meet the stated requirements, it was estimated that a deviation of 15 GHz would be required, the sampling rate would be 800 samples/second, and transmitter AM would have to be limited to less than 5 percent. In general, phase measurements appeared more promising.

### 3.2 Phase Measurement

The basic technique for a phase measurement system is illustrated in figure 3. The distance to the reflecting plane is obtained by measuring the phase ( $\theta$ ) of the received signal relative to that of the transmitted signal. For a signal transmitted at frequency  $f$ , the distance is given by the relationship

$$D = (\theta \cdot c) / (4\pi f). \quad (8)$$

Since the detection of phase between two unmodulated (CW) signals is ambiguous every  $2\pi$  radians ( $\pi$  for a simple mixer/detector), this measurement technique has a limited unambiguous range of detection of  $D_u$  as follows:

$$D_u = c/(2f). \quad (9)$$

An unambiguous range of 40 cm requires operation in the UHF region of the spectrum, which is incompatible with the requirements for critical electron density detection.

If it is assumed that there are no frequency dependent phase shifts (other than propagation delay) in the transmission path (including the reflecting surface), it is possible to make phase measurements at two frequencies and derive the distance from the difference in the two phase measurements. The measurements must be simultaneous unless everything remains stationary during the interval between measurements.

The primary advantages of this phase measurement technique are: 1) the practicality of using unmodulated (CW) sources for the millimeter wave frequencies of interest and 2) the limited spectral width required for the transmitted signal. The primary disadvantage is the requirement of a high signal-to-interference ratio for the primary response at the phase detector. The most damaging error comes from synchronous interference from multiple reflections or spurious signal paths.

## 4.0 Dual Frequency Instrument Configurations

A dual frequency phase measurement technique was chosen for investigation and is illustrated in figure 4. This system uses a reference oscillator that amplitude modulates the carrier to produce a double sideband suppressed carrier (DSBSC) signal. The received signal is processed to detect the difference frequency between the two sidebands and, by means of a differential phase detector, compares the phase of that signal to the phase of the reference oscillator.

Two systems based on this measurement scheme were originally proposed. The frequencies chosen, 24.4 GHz and 220 GHz, are intended to be representative of the low and high end of the range of frequencies corresponding to electron densities expected in the plasma. Figures 5 and 6 are block diagrams of the proposed systems. A difference frequency of 160 MHz was selected because of readily available components.

### 4.1 Single Oscillator System

Figure 5 is a detailed block diagram of the original 24.4 GHz system that was built and tested. The 24.4 GHz transmitter oscillator is modulated by the 80 MHz reference oscillator. A single balanced mixer is used for modulating the carrier, producing a signal consisting of two spectral lines separated by 160 MHz. This signal is filtered and fed to a transmit horn. A directional coupler (not included in the laboratory system) samples the reflected signal received at the transmit horn, which allows the transmitter to also function as a simple reflectometer (reflected power monitor only). This mode is included in the proposed system because the use of separate transmit and receive antennas leaves a blind spot for reflecting boundaries at or just above the antenna ground plane surface. The receive horn feeds the signal through a band pass filter to a mixer where the signal is down-converted to the first IF, 1.6 GHz, and amplified. The signal is then square-law detected (mixed with itself) to recover the 160 MHz difference frequency. This second IF is filtered and amplified, and the amplitude is measured for gain control and for received power information. This signal and the 160 MHz reference are both routed to the phase detector where the phase difference is measured. The outputs of the

phase detector are proportional to the sine and cosine of the phase difference between the inputs. The distance to the reflecting plane can be determined from this phase measurement.

#### 4.2 Two Oscillator System

Two possible configurations for the 220 GHz system are shown in figure 6. Both configurations use two oscillators in the transmitter rather than a single modulated oscillator because available hardware could not provide the required sideband power with a closely controlled frequency separation. The receiving and detection subsystem of both configurations is the same as that of the single oscillator system. Configuration A was originally proposed, however, configuration B was subsequently proposed as a means of eliminating one multiplier and allowing the detection of the difference frequency between the two oscillators to be accomplished in a lower frequency band (desirable due to the availability of detectors). The difficulty with configuration B is that a large number of cross products are generated in the multiplier such that the output consists of multiple spectral lines, separated by 160 MHz. This may not present an interference problem, however, considerable analysis and/or experimentation is required to determine this. At the time of this writing, little more than preliminary work has been done on developing the 220 GHz system. Two 73.3 GHz Gunn oscillators have been locked to track with a 160 MHz difference frequency and their summed output tripled to 220 GHz, but more work is required to obtain the desired output power and spectrum. It was determined experimentally that frequency-locking was more readily obtained than phase-locking. This should be satisfactory if the phase detector reference is derived from a filtered output of the detected difference frequency rather than a reference oscillator.

## 5.0 Single Oscillator, 25 GHz System Development

Testing and development of the 25 GHz system progressed through several stages and ended with the modification of the system to include frequency modulation. The results which follow are organized chronologically to illustrate the path of the development. Initially, the necessary system components were accumulated and each was tested and individually characterized. The system was then assembled, and some testing and adjustment were performed with the transmitter connected directly to the receiver through a variable attenuator rather than via the horn antennas. Next, the system was operated using direct, line-of-sight transmission path between the horns. Finally, the system was set up to measure distance to a reflecting plane in a configuration intended to simulate the operating conditions for MRIS.

### 5.1 Initial Development and Evaluation

Components were acquired, with the exception of the directional coupler and the reflected power detector, to build the 25 GHz single-oscillator system as shown in figure 5. Most of the components were standard catalog items that were readily available. As shown in figures 5 and 6, the receiver section from the first 1.6 GHz IF to the phase detector output are identical for both the 25 and 220 GHz systems. Only the RF and reference oscillator sections are different. A laboratory breadboard was assembled in the configuration of figure 5, excluding the reflected power detector and coupler.

Initial system testing was conducted with the transmitter connected to the receiver with waveguide through a variable attenuator. The system was tested to determine and improve dynamic range, assess the value of AGC, measure noise performance, to measure phase error (i.e., error in the phase angle as determined from the sine and cosine outputs of the phase detector), and determine the sources of the phase error.

Figure 7 shows the measurements of video output and phase error as a function of input power for a system configured with a fixed gain of 45 dB for the 160 MHz IF amplifier and 14 dB gain for the 1.6 GHz IF amplifier. The video

output is the detected amplitude output for the 160 MHz amplifier of figure 5. As can be seen in figure 7, the phase error for input levels less than -45 dBm becomes unreasonably large. The dynamic range of the system, where the phase error is small, is approximately 35 dB, which is adequate.

The maximum level of phase error that can be tolerated is determined from the required distance measurement accuracy, given as  $\pm 1$  cm to the reflecting plane in the plasma. Analysis indicates that the average group velocity in the plasma can be assumed to be about one-half that of free space. For a 160 MHz difference frequency, the average differential phase shift is 3.8 electrical degrees per cm. Since a unit change in transmission path length corresponds to a half-unit change in the distance to a reflector, a  $\pm 1$  cm round trip distance variation in the plasma corresponds to a phase shift of  $\pm 7.6^\circ$ . The phase measurement error should be less than this to allow for an error contribution from the analysis of the flight data. As indicated earlier, the selection of 160 MHz was based largely on component availability. A higher modulation frequency could provide a higher detector sensitivity (deg./cm). For example, the phase shift corresponding to  $\pm 1$  cm at 250 MHz is  $\pm 12^\circ$ .

An automatic gain control (AGC) was applied to the second IF amplifier (160 MHz) in order to increase the dynamic range of the receiver. The phase shift introduced in the second IF amplifier varied considerably with the applied AGC voltage. Figure 8 shows the total phase error and video voltage versus input power. The contributions from other sources of phase error in the signal path were found to be small compared to the error introduced by the IF amplifier, so a phase-compensated voltage controlled attenuator in the IF would be a better option for gain control. An algorithm was developed to correct the phase detector outputs, sine and cosine, receiver phase error. The algorithm uses the video, sine, and cosine output voltages to produce corrected phase and input power level measurements. The algorithm is based on a simple exponential fit to the measured phase error versus video output.

With the AGC loop installed, fixed paths corresponding to  $0^\circ$  and  $45^\circ$  between the transmitter and receiver were measured at varying power levels. Comparison of figure 9 with figure 7 reveals the AGC added about 15 dB to the

dynamic range. The error is less than  $\pm 5^\circ$  for a dynamic range greater than 50 dB.

#### 5.1.1 Direct Transmission Tests

The first system tests using antennas were conducted over a direct path with the transmit and receive horns aimed directly at each other. No ground or reflecting planes were used. The transmitter was placed on a fixed mount and the receiver on a mobile mount and positioner. A stable table was used to isolate the apparatus from physical vibration. For these tests, the sine, cosine, and video outputs were measured versus distance between the horn antennas, and the data were processed using the previously discussed algorithm.

Distance measurements were made as the receiving antenna was moved from 0 to 48 inches (0 to 122 cm) in 3-inch increments. Processed phase angle measurement data versus distance was compared with an ideal phase angle versus distance slope characteristic with good results. From about 10 cm to 120 cm, the accuracy was  $\pm 5^\circ$  or better (standard deviation for the entire range of distance was  $2.3^\circ$ ), which is well within the desired limits. The error increased noticeably as the antennas approached each other (distance less than 10 cm). This systematic error is believed to be a consequence of interference from reflections off the faces and cones of the antennas.

#### 5.1.2 Reflected-Path Tests With No Ground Plane

The test setup used for distance measurements to a reflecting plane is shown in figure 10. The transmitter and receiver horns were mounted together on a fixed mount with the apertures in the same plane. The initial tests did not include a ground plane around the antennas. An 18 by 18-inch reflecting plate was mounted parallel to the plane of the horns on a mobile mount and positioner for use as a target, and distance measurements were made from the plane of the horns to this reflecting plate. In this configuration, tests were conducted using two antenna spacings, various reflecting plate tilt angles, different reflecting plate sizes, and absorber around the apparatus.

The most significant result from these tests was that the magnitude of the phase error was greater than that for the direct transmission tests, and the magnitude of the phase error was largely independent of the test conditions. For example, with an antenna spacing of 2 inches and no absorber material used around the test apparatus (for distances from 7 cm to 60 cm), the standard deviation for the phase data is 5°. This error magnitude is more than twice that of the direct transmission measurements.

Phase error increased rapidly as the distance was reduced from 7 cm. Some degradation was expected because the antenna beamwidth (3 dB) of 30° does not allow coverage of this region. As the spacing is reduced, the signal received from the first reflection is no longer the predominate signal.

An effort was made to identify the cause of the increase in error over the direct transmission tests. An absorber tunnel was built to enclose the antennas and reflecting plate in order to eliminate the possibility of unwanted reflection surfaces. Measurements for this setup showed the same level of phase error and indicated a definite periodicity in the phase error data. Since the frequency associated with the period of the error did not correspond to the modulation frequency (or any harmonic or subharmonic), the sampling increment (delta distance) was reduced to eliminate the possibility of aliasing. Data were collected over short distance segments (a few centimeters) with samples taken every 0.1 cm. The results indicated a complex interference pattern with a basic period of 0.6 cm, or a half wavelength at 24.4 GHz. This behavior suggested that the phase error was caused by interference from spurious paths between the transmitter and receiver. Sources considered were direct coupling between the horns, multiple reflections, and internal coupling between the transmitter and receiver due to poor isolation. After additional testing, it was concluded that this interference was primarily from multiple reflections between the antenna faces and the reflecting plate.

### 5.1.3 Reflected-Path Tests With a Ground Plane

A small ground plane was added to the antennas (figure 10), and testing was resumed using small sampling increments (0.1 cm or less). As expected, the phase error was considerably increased relative to the test with no ground

plane. This increase in phase error was due to the occurrence of multiple bounces between the ground plane and the reflecting plane. Analysis showed that the complex interference pattern measured was consistent with that expected for a Fabry-Perot resonant cavity, which is formed by parallel reflecting planes. In figure 11, the measured data are superimposed on calculated data produced by a numerical model (Ref. 3). The numerical model assumes infinite ground and reflecting planes with circular waveguide apertures in the groundplane. The electromagnetic fields between the two surfaces are computed, so that the signal coupled to the receiving aperture can be determined. A phase offset was added to the calculated data to aid in the comparison (i.e., to align the waveforms). The fine variations in the experimental data are believed to be the result of edge diffraction and other perturbations from the use of finite ground and reflecting planes. The salient feature of the data is that the phase error is unacceptably large and exhibits a periodicity of a half wavelength at the carrier frequency of 24.4 GHz. Agreement between the calculated field data and the measured data indicated that the source of the phase error was multiple, unattenuated reflections between the plates.

The first effort initiated to deal with the problem of multiple reflections involved placing pyramidal absorber over the ground plane. This had the effect of attenuating the unwanted reflections. Significantly, it was found that the error could only be reduced to previous levels (with no ground plane) if the entire ground plane was covered. When only a small portion of the ground plane was left uncovered, error increased significantly. It appeared that while it might be possible to modify the TPS to include absorbent material, this material would have to have broadband properties, provide 16 dB or more attenuation (per reflection), and possibly cover a large area of the aerobrake on the AFE. Although such changes to the TPS may be possible, they do not appear practical since any new material would have to be developed and qualified, and the potential for out-gassing and flow field pollution would have to be examined.

A parallel effort was initiated to redesign the system to provide immunity to the effect of the multiple reflections. It was theorized that the integral of phase over a number of periods of this interference pattern would effectively

suppress the interference. This could be accomplished experimentally by varying the carrier frequency at a fixed reflector distance.

## 5.2 Modification and Evaluation With Frequency Modulations

The computer model was expanded in order to investigate the possibilities associated with frequency modulating the DSB signal. It was modified to iterate through a finite number of frequency steps and to compute the average of either the resulting sine and cosine of the phase, or the computed phase angle. This allowed the effects of frequency modulation of the carrier to be compared with experimental results.

### 5.2.1 FM Implementation and Tests

Frequency modulation was implemented by synchronously modulating the transmitter carrier oscillator and the receiver local oscillator, as shown in figure 12. The system modeling program indicated that a peak deviation of  $\pm 1$  GHz was necessary to reduce the phase error to an acceptable level (Sec. 5.4). The Gunn oscillators previously used for the carrier and the LO could not be modulated to this extent, so the system was evaluated using available laboratory test equipment. A pair of laboratory synthesizers, locked with the appropriate frequency separation, was used as signal sources. The sine and cosine outputs from the phase detector were applied to integrators (analog filters) with a 0.1 second time constant. Center-to-center antenna spacing for this test was 2.0 inches (5.08 cm). Distance measurements were made with the swept carrier system from 5 to 61 cm (to the reflecting plate) in small distance increments. At each discrete distance, the sources were continually stepped through 100 frequency steps for a total deviation of  $\pm 1$  GHz while the detector outputs were integrated. Figure 13 shows the resulting measured phase angle versus the distance to the reflector. Figure 14 shows the distribution of the absolute magnitude of the phase error and indicates the accuracy of the measurement. For the 160 MHz difference frequency, 82 percent of the data are within the desired accuracy of  $\pm 7.6^\circ$ . Note that for an assumed difference frequency of 250 MHz, 96 percent of the data points are within  $\pm 12^\circ$ , the desired accuracy. Although this simple extrapolation of the

experimental results has not been tested, a larger difference frequency would be desirable for future development.

Another set of measurements was made with center-to-center antenna spacing reduced to 1.24 inches (3.15 cm), and the phase angle measurements are shown in figure 15. This spacing was the minimum physically allowable for the 1-inch inside-diameter horns. For the antennas used, this spacing probably resulted in the maximum direct-coupling level that would be attained for parallel mounting. Comparison of the distance measurements from 0 to 10 cm for figures 13 and 15 shows that the closer spacing provides better performance in this region. Notice that the phase-angle slope begins falling off at distances less than about 10 cm in figure 13, whereas the slope in figure 15 does not start to fall off until less than 5 cm. Also, a corresponding reduction in received signal strength occurs at approximately 5 cm, as indicated in figure 16.

Measured phase-error characteristics (with antenna spacing at 3.15 cm) are shown in figures 17, 18, and 19. Figure 17 gives the phase error as a function of distance to the reflector over the entire 60 cm range. Figure 18 provides a distribution of the phase error data, and figure 19 provides a cumulative distribution of the absolute magnitude of the phase error data. As can be seen, 90 percent of the data points fell within  $\pm 12$  degrees.

Additional measurements were taken, with small steps in range, from 10 to 20 cm and 30 to 50 cm, with frequency deviations of 0.7 GHz, 1.0 GHz, and 1.4 GHz. The results are shown in figures 20, 21, and 22, which provide a detailed view of the fluctuations in the error. These results were surprising in that they did not show a reduction in error with increased deviation. The best performance was obtained with the lowest deviation (0.7 GHz). This is discussed further in Section 5.4.

### 5.3 Computer Model Comparison

#### 5.3.1 Model Description

The latest system computer model assumes far-field antenna characteristics and ideal reflectors with the exception of an attenuation (an input parameter to the model) associated with the reflection from the antenna ground plane (or vehicle surface) and computes a vector sum of the received signals due to any number of reflections between the surfaces plus a direct (between antennas) coupled signal. It does not account for the existence of the antenna apertures in computing the signal reflected from the ground plane back to the target surface. Therefore, it is not expected to provide a good analytic tool at standoff distances below approximately 4 to 6 cm. This model does, however, simulate the full system, with control over the system parameters, as indicated by the parameter list on the figures (see fig. 31). When used to simulate operation in a plasma, it doubles the transmission time delay computation and applies an excess path attenuation factor (a model input parameter) to the total path distance of each signal component. (Based on results from a model of wave propagation in plasma, a useful estimate for the average wave velocity in plasma was found to be  $c/2$ . This model also provided estimates for attenuation within the plasma.) The input parameter list is self explanatory, however, it should be pointed out that the XMIT PWR input is the power in each sideband (total transmit power is 3 dB higher), the REC NOISE input is the required input signal level to obtain a 0 dB SNR at the input to the phase detector, and the two FM LIN inputs are the coefficients of the second and third order nonlinear terms, respectively. The model can be run in two modes. In the first mode, it averages the sine outputs and cosine outputs of the detector independently over the period of the FM sweep and then computes the output phase. In the second mode, it computes a phase angle continuously, from the sine and cosine outputs, and averages this computed phase angle over the period of the FM sweep. In the second mode, it employs an algorithm, based only on detected output values, to minimize the possibility of encountering the phase discontinuity existing at  $\pm 180^\circ$  during the integration.

### 5.3.2 Comparison of Model and Experimental Data

The model has been useful in both identifying sources of error in the experimental data and evaluating the effect of design modifications (i.e., the use of FM) prior to hardware implementation. The agreement between experimental and analytical data is exemplified by figure 23, a case with no frequency modulation. Figures 24 and 25 compare a case with frequency modulation of  $\pm 0.7$  GHz with test results (previously shown in figures 20 and 21). Results using the model with two other FM deviations did not agree as well with experimental results (figures 20 and 21 for deviations of  $\pm 1.0$  GHz FM and  $\pm 1.4$  GHz FM). In both cases, the magnitude of the phase errors from the experiment were approximately 3 to 4 times as large as those from the model run. This is currently being investigated and is discussed in the next section. Figure 26 illustrates the agreement between the model prediction of the signal strength and the experimental data from the test dated 7/25/88 (shown in figures 15 and 16). The disagreement in the region below a standoff distance of 7 cm is indicative of the model deficiencies. The antenna aperture for this run was reduced to 1.9 cm to match the measured gain of the antennas. A difference of approximately 2 dB still exists, which is probably due to the initial receiver calibration. Although data are not presented here, another area of agreement between analytical and experimental data is that the model predicted the rather abrupt discontinuity in the phase/distance characteristic occurring at approximately 3 cm, as shown in figure 15.

### 5.4 Discussion of Results to Date

The use of frequency modulation to reduce phase error was investigated experimentally and analytically. Sine and cosine averaging was used to estimate the average received phase for the experimental evaluation because the laboratory apparatus would not support phase averaging. (A discussion of sine and cosine versus phase averaging follows in this section.) Analytic results using sine and cosine averaging, figure 27, show the predicted phase errors (i.e., deviation from a straight line phase/distance characteristic) as a function of range and frequency deviation. Although the -60 dB antenna decoupling parameter with the horns almost touching was unrealistic (current indications are approx. -46 dB), these plots show a general reduction

of phase error as deviation was increased, with an acceptable level at approximately 1 GHz deviation.

The disagreement between the experimental and analytical data with frequency deviations of 1 and 1.4 GHz may have been due, in part, to nonlinearity in the modulation for wider frequency deviations. Model runs were made with the nonlinear modulation, characteristics shown in figure 28, at a deviation of 1 GHz. The comparisons of these simulations with experimental data are shown in figures 29 and 30. Although these comparisons are favorable, the linearity of the modulation has not been directly measured.

To compare the use of phase versus sinc/cosine averaging, model runs were made with the same nonlinearity (fig. 28). Phase averaging provided nearly a 2:1 reduction in the peak-peak phase error over sinc/cosine averaging as shown in figure 31. With better linearity in the frequency modulation, the reduction factor should be greater. This could be implemented in a digital form with a look-up table for the arc-tangent function and a digital processor for the integration. A side benefit in doing this is that the amount of measured data that must be stored onboard the AFE vehicle would be reduced by approximately one-third.

An interesting possibility for the instrument design is the use of dual modes of operation (bistatic and monostatic) to provide good coverage at both short and long ranges. This could be implemented with the addition of a circulator and an RF switch. The obvious reason for lack of coverage at short ranges is the displacement of the two antennas. A model for monostatic operation was developed, and a series of runs were made to illustrate the performance in both modes. Figures 32 through 35 illustrate the predicted performance of the two modes. These runs were made with a DSBSC amplitude modulation resulting in two spectral lines separated by 250 MHz, which is then frequency modulated with a ramp function over  $\pm 1$  GHz. An excess path attenuation of 0.25 dB/cm was used, to give a path attenuation of 15 dB at 30 cm. The circulator isolation assumed in the monostatic mode was 30 dB, and the total antenna decoupling assumed in the bistatic mode was 50 dB. The nonlinearity attributed to the frequency modulator is shown in figure 36.

Figures 32 and 33 were run with the far-field model and illustrate bistatic performance. The system fails for distances less than about 3 cm. Also, the predictable phase ambiguity at  $360^\circ$  can be seen at 30 cm, and the effects of receiver thresholding appear at approximately 32 cm. The received signal strength is shown in figure 33, indicating a required dynamic range of at least 35 dB and preferably 45 to 50 dB. Comparable results using the monostatic model are shown in figures 34 and 35. It can be seen that monostatic performance is good to about 7 or 8 cm, with thresholding occurring at about 9.5 cm. (The threshold mechanism, in both modes, consists of the receiver being captured by the direct coupled signal. The basic receiver threshold, due to thermal noise, is in the region of -55 dBm.) Received signal strength could be used to select the appropriate operating mode to obtain the best measurement over the entire distance range.

## 6.0 Conclusions

The results of this study indicate that a reflectometer can be developed to provide a measurement of the ratio of transmitted to reflected power and a measurement of propagation time over a range from 0 to  $4 \cdot 10^{-9}$  seconds with an accuracy of less than  $\pm 1.3 \cdot 10^{-10}$  seconds. This can be accomplished with the simpler single oscillator system at 25 GHz and possibly as high as 90 GHz or more. There are two problems encountered as the frequency is increased. The first is the reduction in the receiving antenna aperture with increased frequency as the aperture is scaled to maintain a fixed beamwidth. To go from 25 to 90 GHz, the aperture radius is scaled by a factor of 1/3.6 resulting in approximately 11 dB additional loss due to the reduced aperture area. The second problem is the expected increase in the excess path loss. Current estimates are that this loss may be as high as 33 dB at a standoff distance of 30 cm when operating at 90 GHz. This translates into significant changes in system requirements. First, the receiver threshold due to thermal noise must be reduced (or transmitted power increased). A significant reduction in the receiver threshold (i.e.,  $\leq -80$  dBm) is not unreasonable with the use of a narrow-band technique. Second, the antenna coupling must be maintained at a very low level. At 25 GHz, the system can tolerate 45 to 50 dB antenna decoupling; whereas at 90 GHz, the system will require approximately 75 dB antenna decoupling for the same beamwidth antennas. Of course, any or all of this differential can be eliminated by the use of higher gain antennas (narrower beamwidths), however, this results in other problems such as larger errors or loss of coverage at the closer ranges. A parametric study is required, along with refined estimates of the excess path loss, to define the optimum system configuration (antenna gain and spacing, transmitted power, etc.) at the higher frequencies.

## 7.0 Continuing Efforts

This Feasibility Study has demonstrated experimentally that distance measurements to a reflecting plane can be made with sufficient accuracy to be useful to scientists investigating the flowfield of a reentering spacecraft. Subsequent to this study, NASA will continue an investigation of the instrument design and data analysis, both experimentally and analytically. The design and construction of the flight instrument will be contracted, and the instrument contractor will be required to conduct a definition study to investigate various options for the design including but not be limited to the scheme used here. Task areas subject to further investigation are as follows:

- 1) Develop and experimentally verify a computer model for simulation of the instrument operating at close ranges to the reflecting surface.
- 2) Conduct parametric studies, using the computer models, for the system design (transmitter power, antenna size and spacing, modulation, etc.) required for optimum performance at higher carrier frequencies.
- 3) Refine the basic detector design using computer models and experimental measurements for verification. This will include implementation of phase averaging in the experimental system.
- 4) Continue the design, development, and evaluation of techniques and hardware required to obtain the desired transmitted signal format at higher carrier frequencies.
- 5) Investigate the TPS characteristics to determine the loss tangent and dielectric constant as a function of temperature and frequency.
- 6) Continue studies of potential dynamic behavior of the plasma and any resulting effects (e.g., Doppler-shifted signals).
- 7) Investigate techniques and develop software required for post-flight data analysis.

## List of References

1. Jordan, E. C., and Balmain, K. G.: Electromagnetic Waves and Radiating Systems. Second ed. Prentice-Hall, Inc., Englewood Cliffs, NJ, 1968.
2. Skolnik, M. I.: Introduction to Radar Systems. Second ed. McGraw-Hill, United States of America, 1980.
3. Bailey, M. C.: CWG - A FORTRAN Program for Mutual Coupling in a Planar Array of Circular Waveguide-Fed Apertures. NASA TM-101614, June 1989.

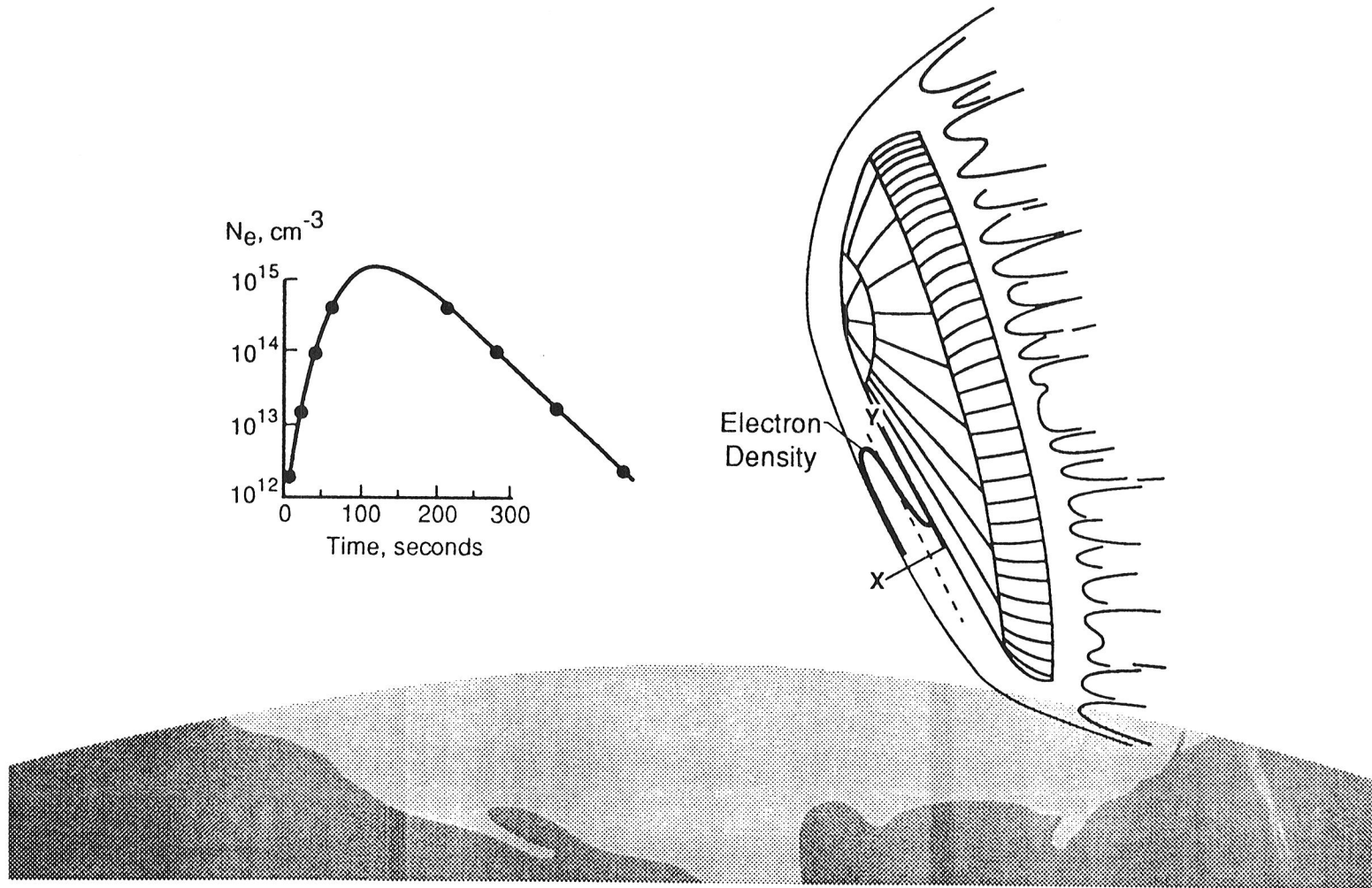


Figure 1. Illustration of the Microwave Reflectometer Ionization Experiment (MRIS).

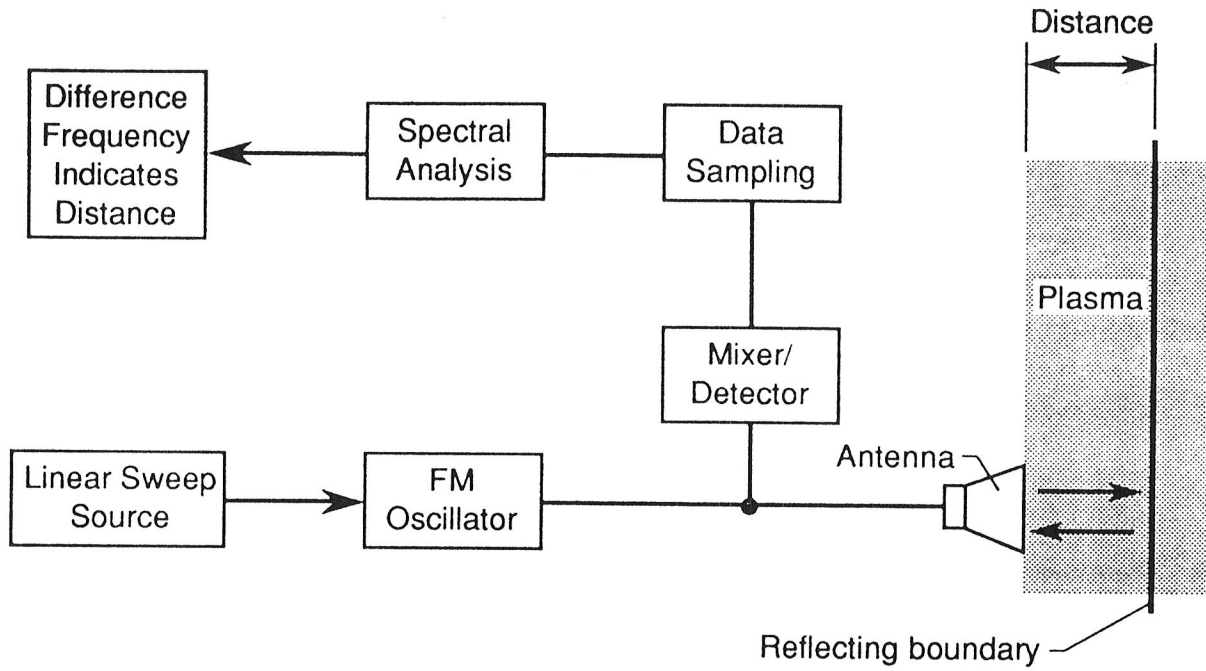


Figure 2. Frequency measurement scheme.

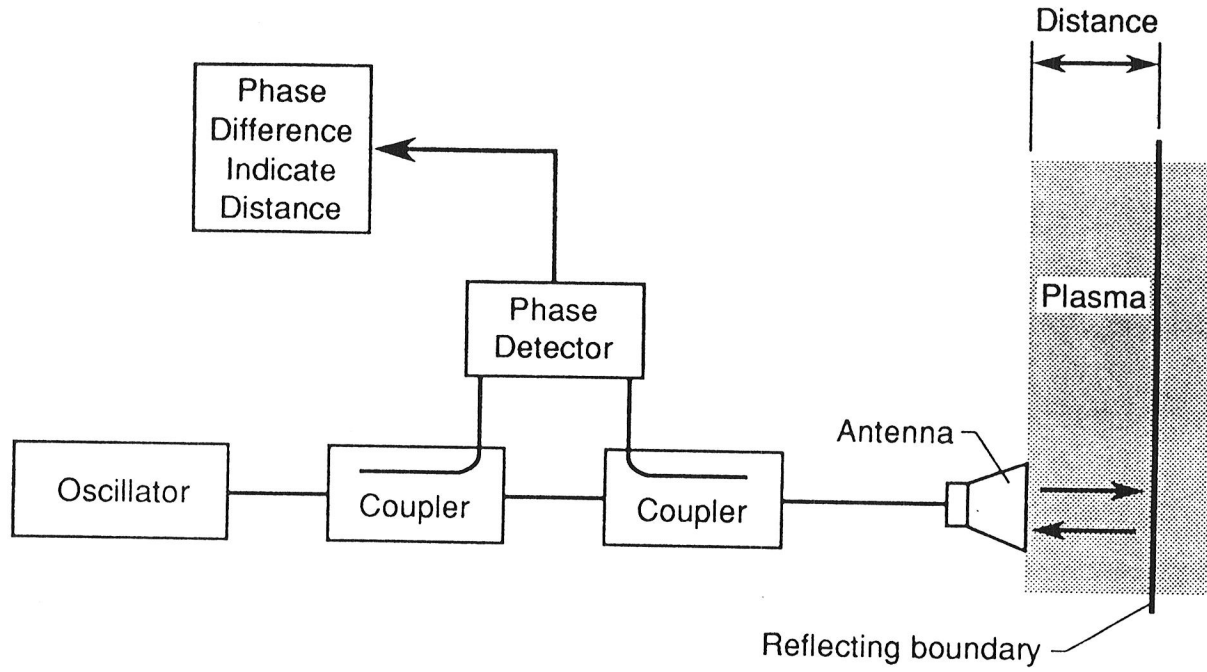


Figure 3. Basic phase measurement scheme.

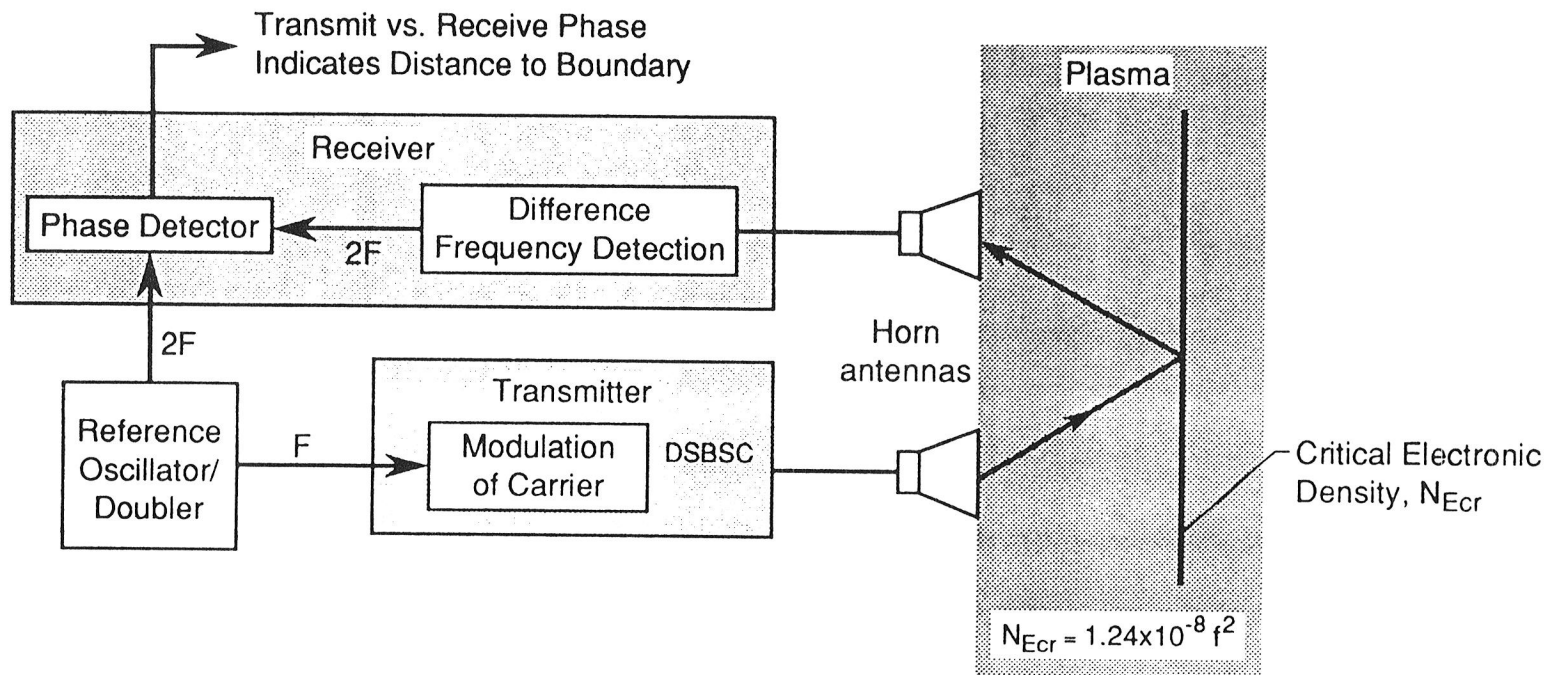


Figure 4. Dual frequency phase measurement scheme.

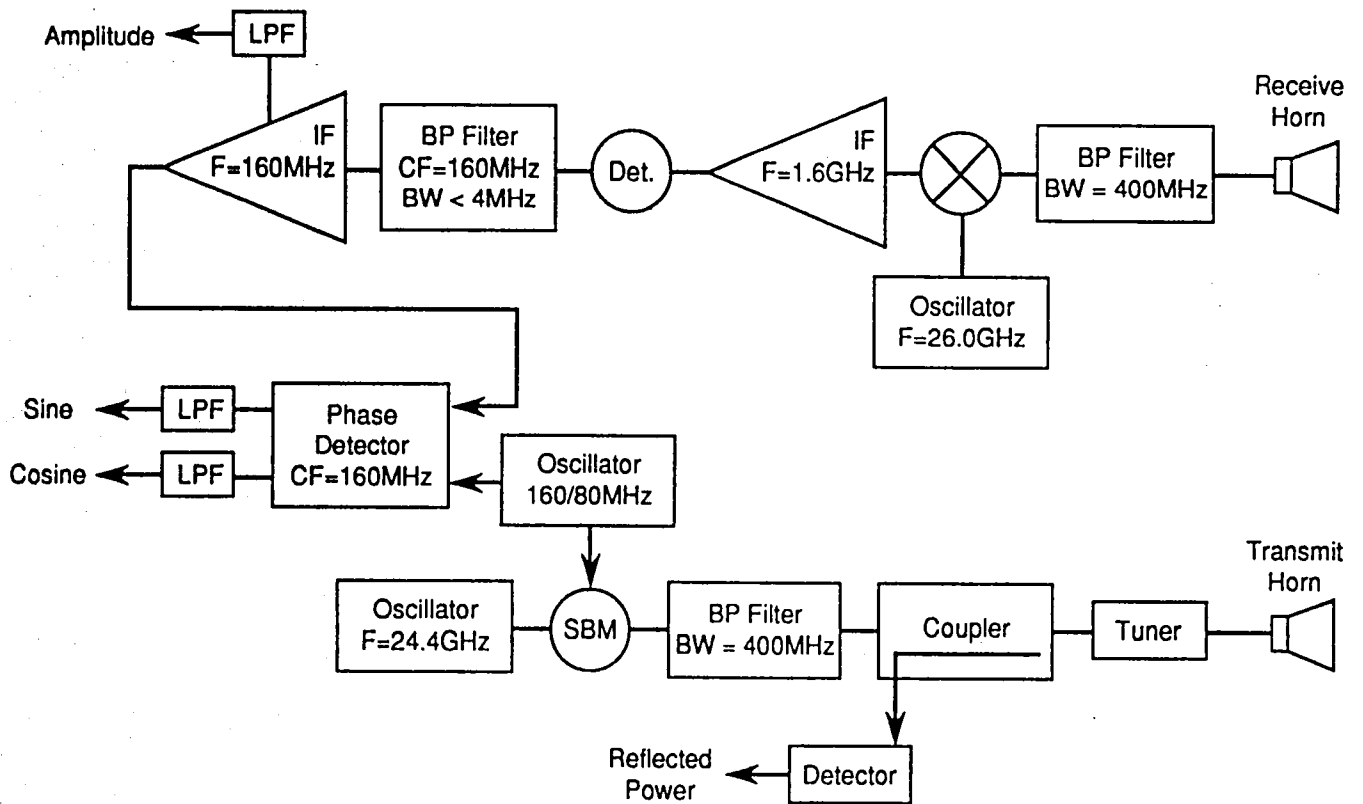
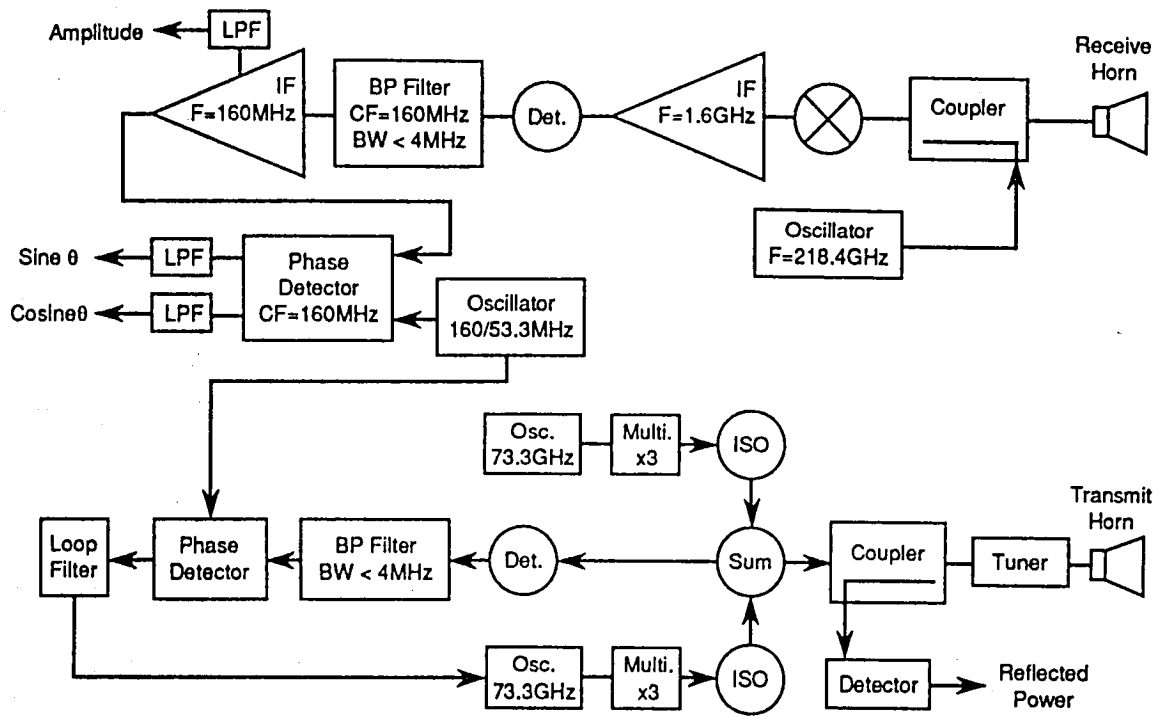
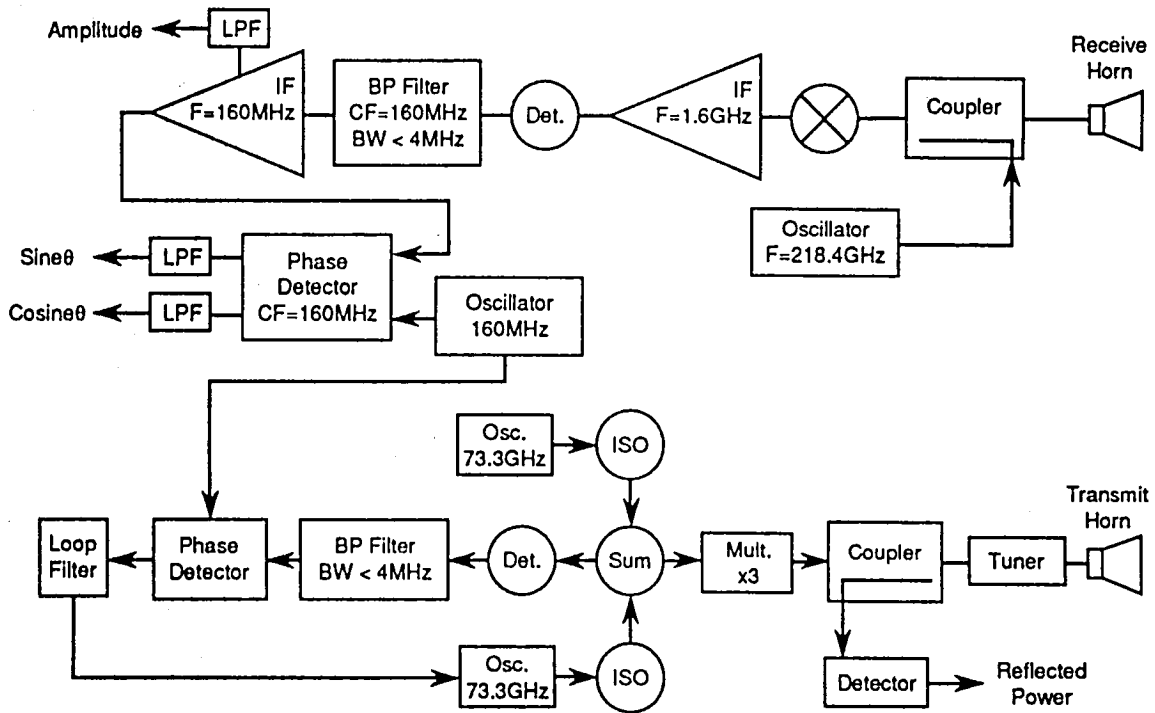


Figure 5. Single oscillator system.



(a) Configuration A



(b) Configuration B

Figure 6. Configurations for two-oscillator system.

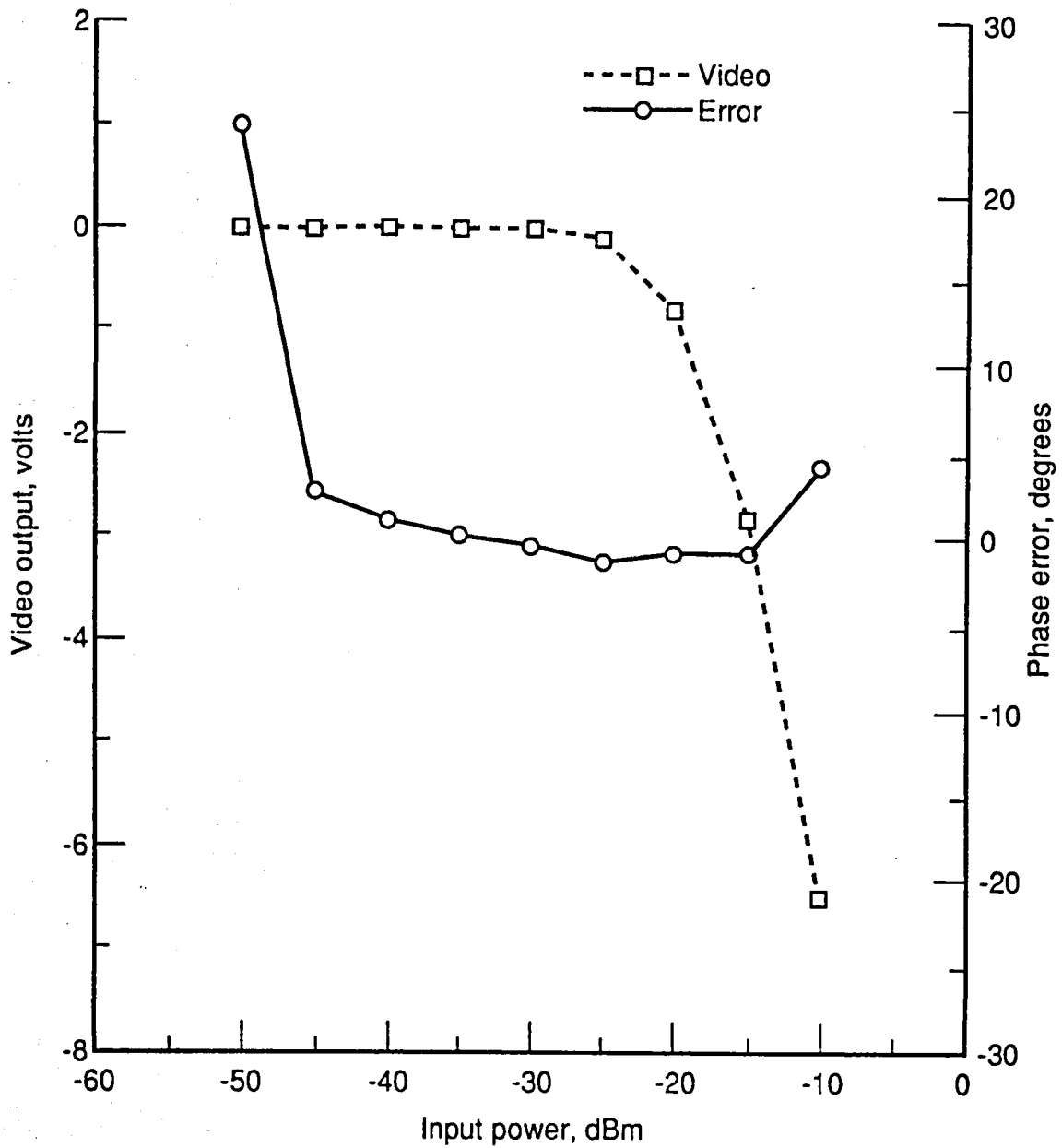


Figure 7. Video output and phase error vs. input power (160MHz gain = 45 dBm, 1.6 GHz gain = 14dB).

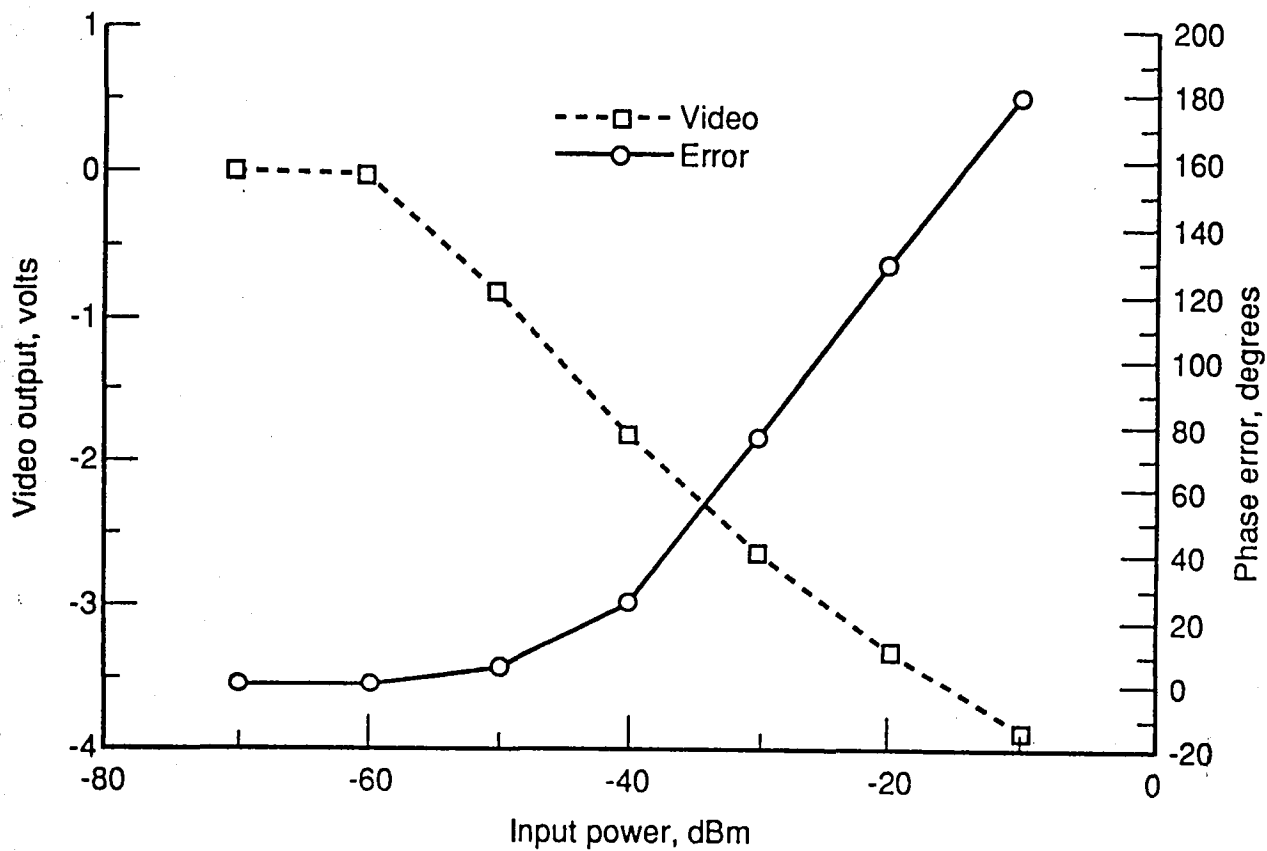


Figure 8. Video output and phase error vs. input power with AGC (1.6GHz gain = 32dB).

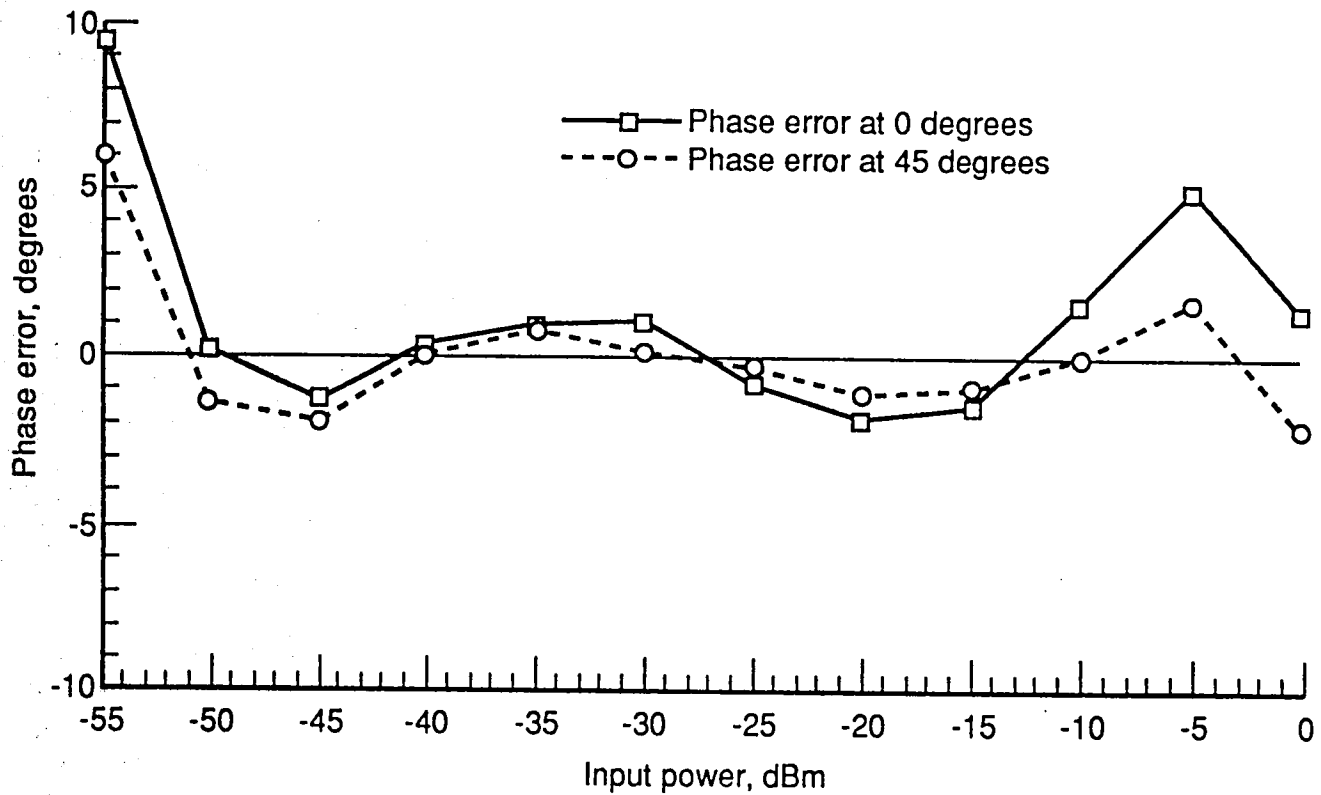


Figure 9. Phase error vs. input power for fixed 0 and 45 degree paths using AGC, and the correcting algorithm.

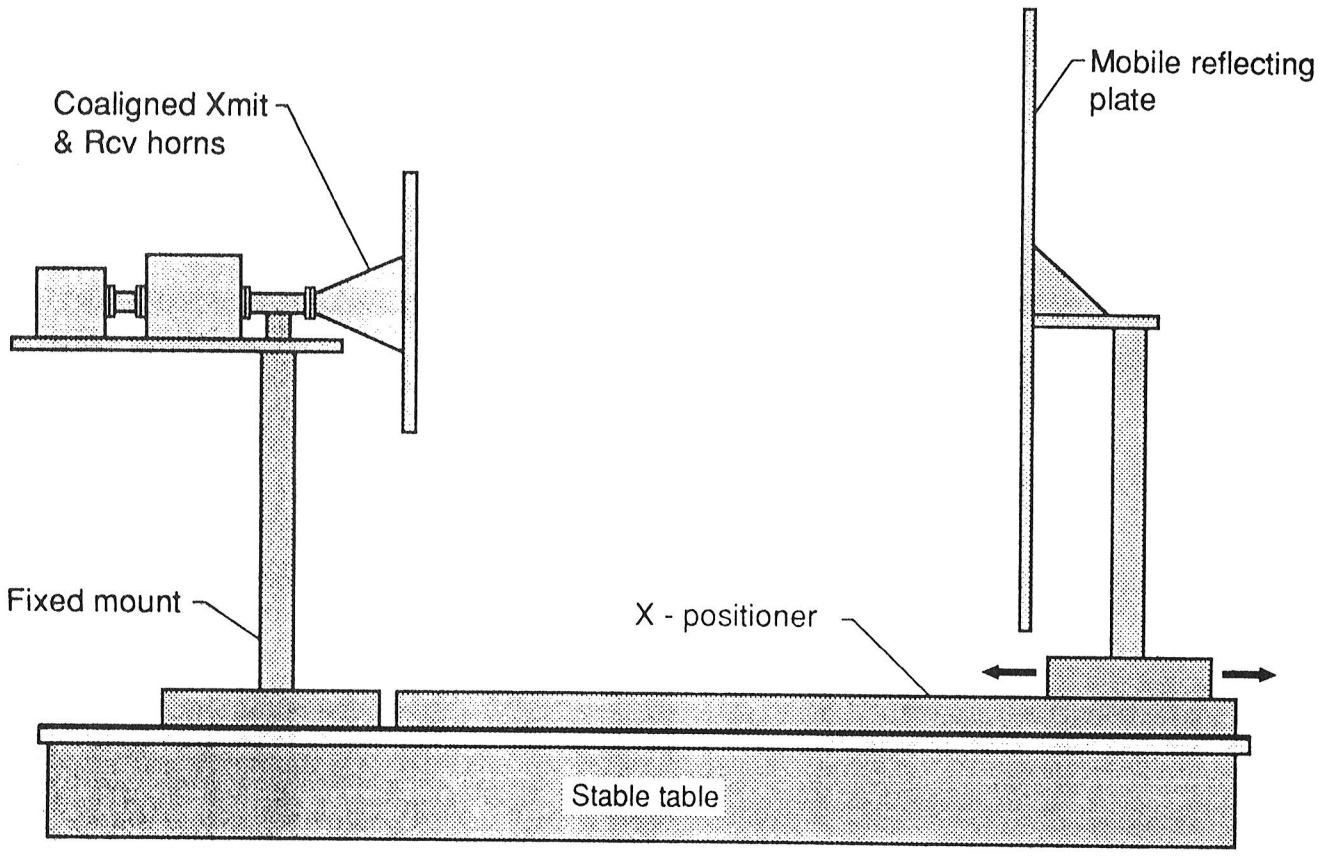


Figure 10. Test setup including a ground plane.

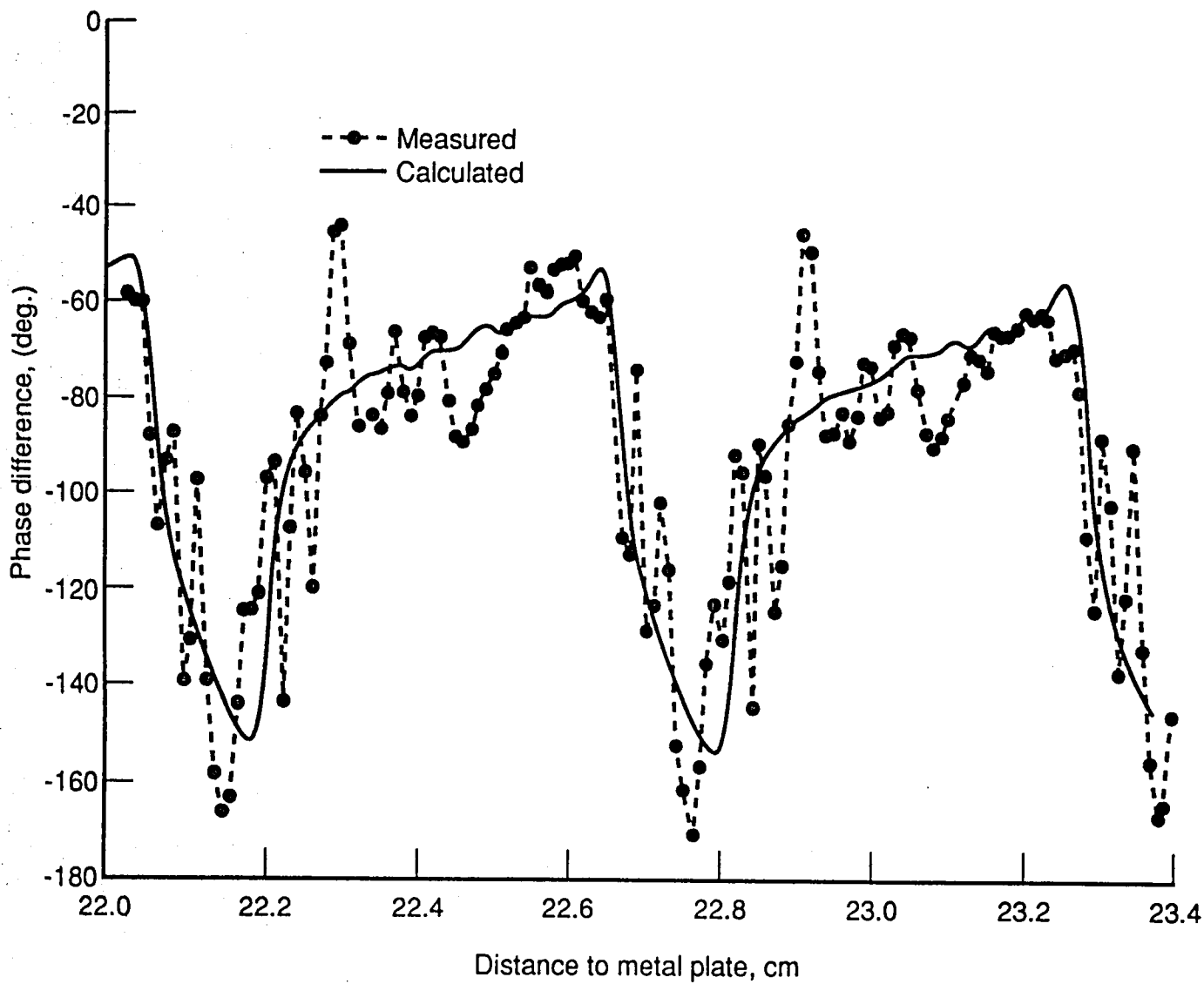


Figure 11. Comparison of measured and calculated differential phase angle at 24.4GHz over the distance range of 22.0 to 23.4 centimeters.

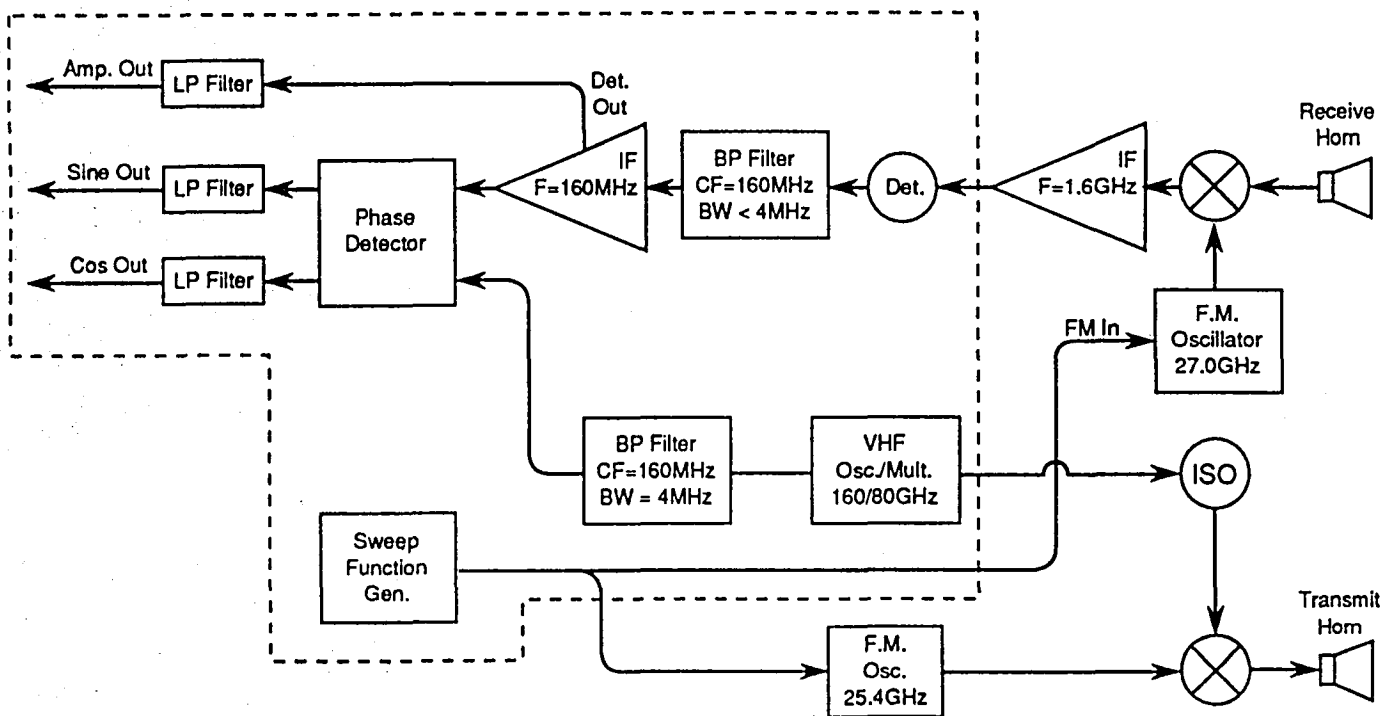
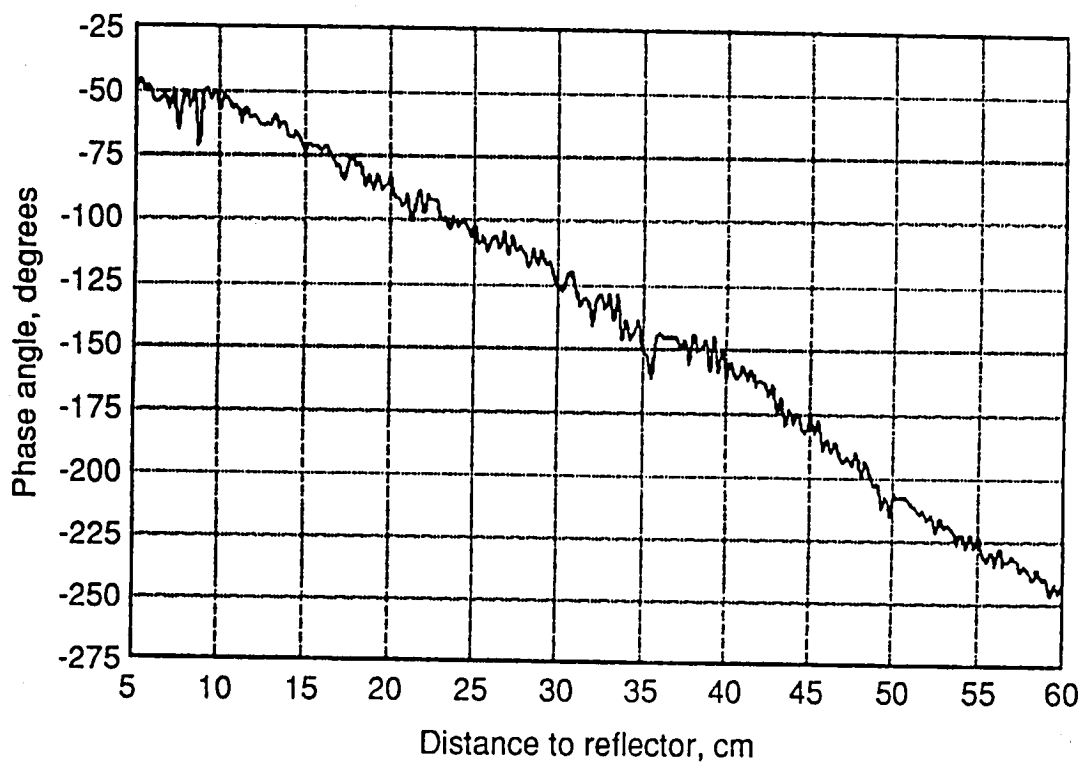


Figure 12. Frequency modulated single oscillator system.



Sine-cosine averaging

**Test Conditions:**

Carrier freq. = 25.4GHz, AM freq. = 80MHz, Peak FM dev = 1GHz,  
 Xmit power = 3dBm, Ant. Dia. = 2.54cm, Ant. tilt = 0°, Ant. spacing = 5.08cm,  
 Ground plane = 12 x 12 inches, Reflection plane = 18 x 18 inches.

Figure 13. Measured phase angle as a function of distance.

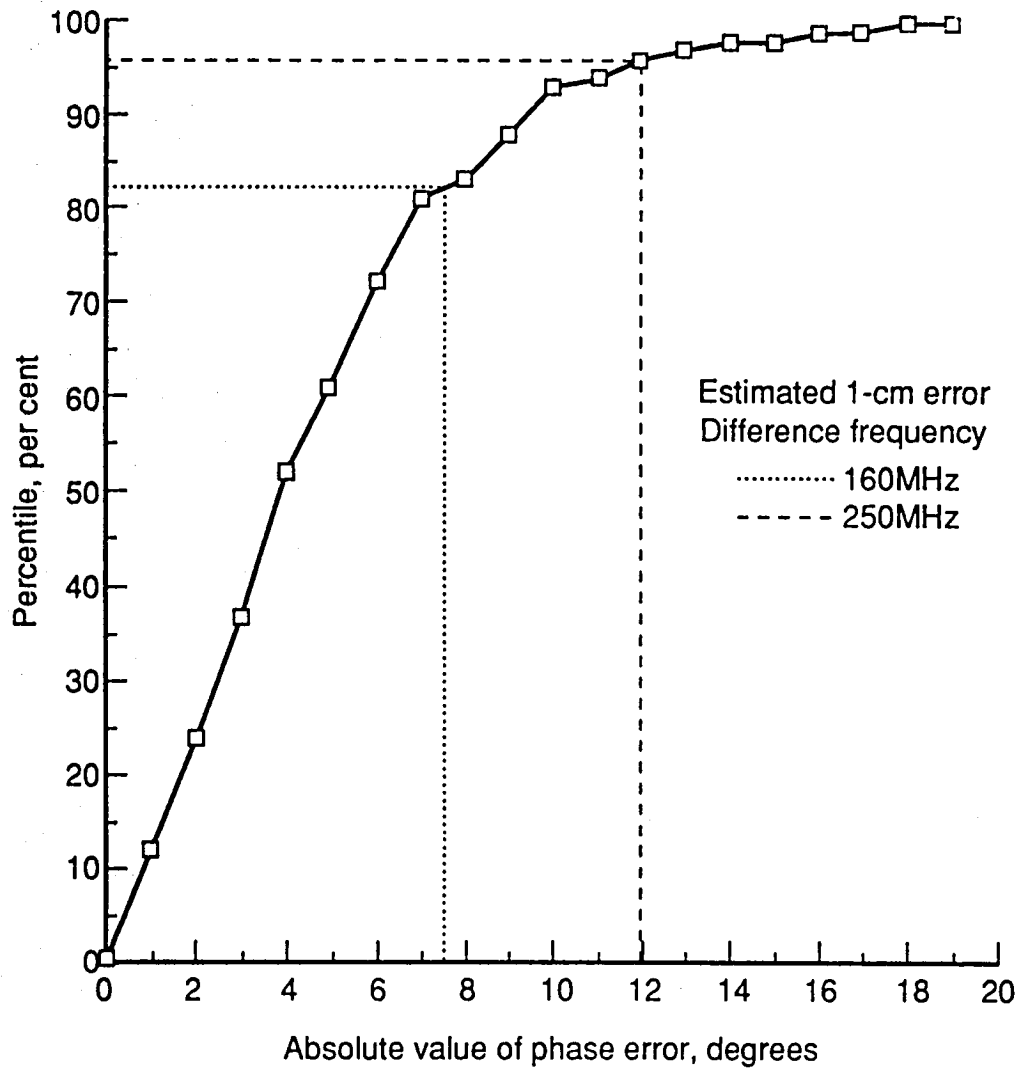
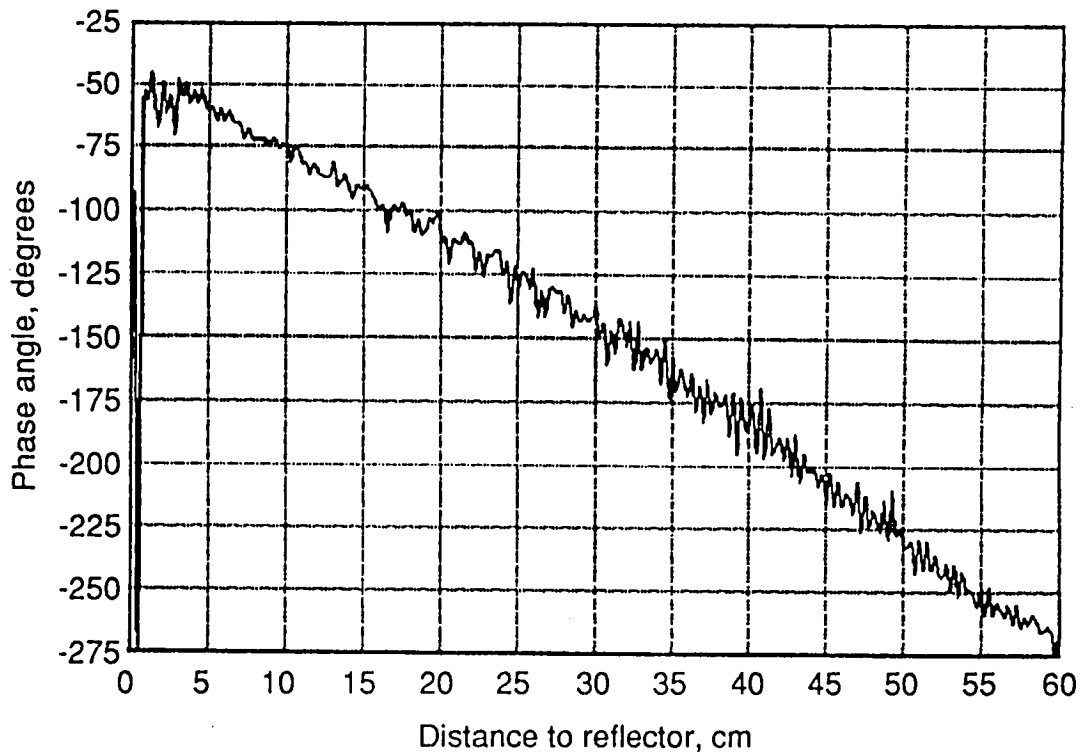


Figure 14. Phase error distribution for the FM system.

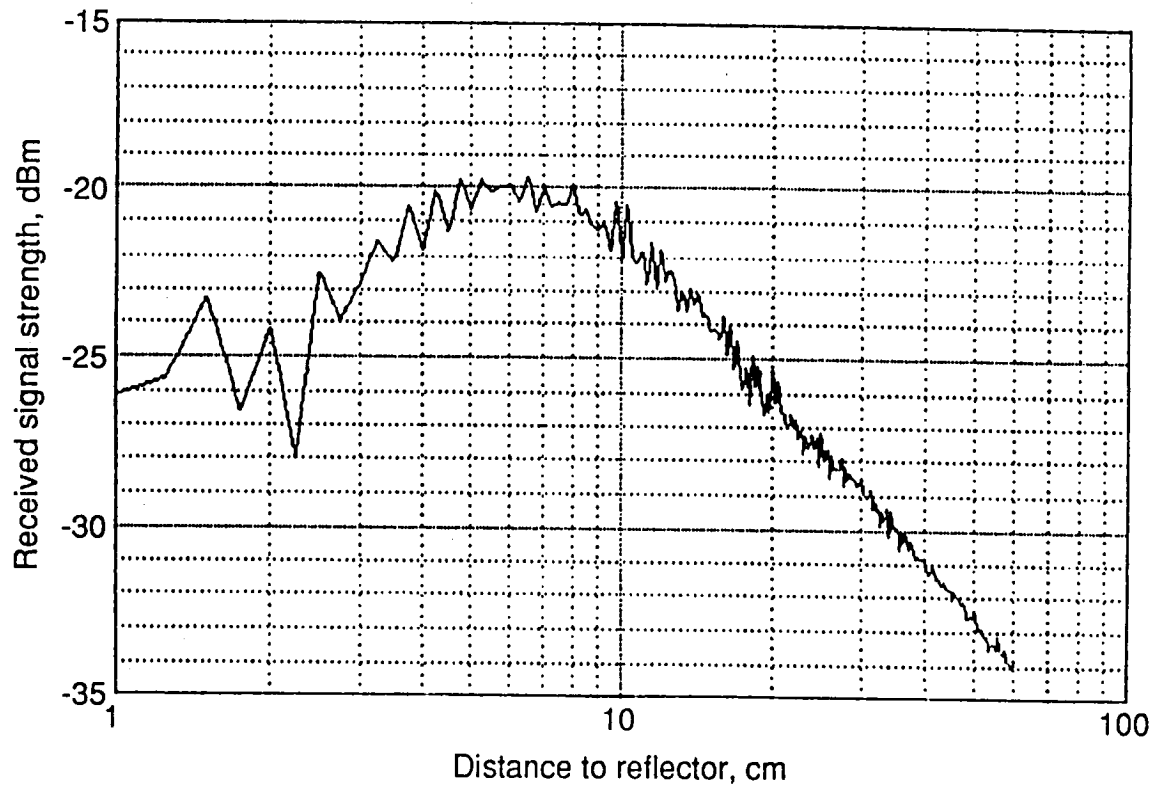


Sine-cosine averaging

**Test Conditions:**

Carrier freq. = 25.4GHz, AM freq. = 80MHz, Peak FM dev = 1GHz,  
 Xmit power = 3dBm, Ant. Dia. = 2.65cm, Ant. tilt = 0°, Ant. spacing = 3.15cm,  
 Ground plane = 18 x 18 inches, Reflection plane = 18 x 18 inches.

Figure 15. Measured phase angle as a function of distance.



Carrier frequency: 24.4 - 26.4GHz  
 100 steps, 5ms dwell time  
 Antennas: 2.65cm diameter  
 3.15cm center-to-center separation  
 Ground plane: 18 x 18 inches  
 Reflection plane: 18 x 18 inches

Figure 16. Measured signal strength as a function of distance.

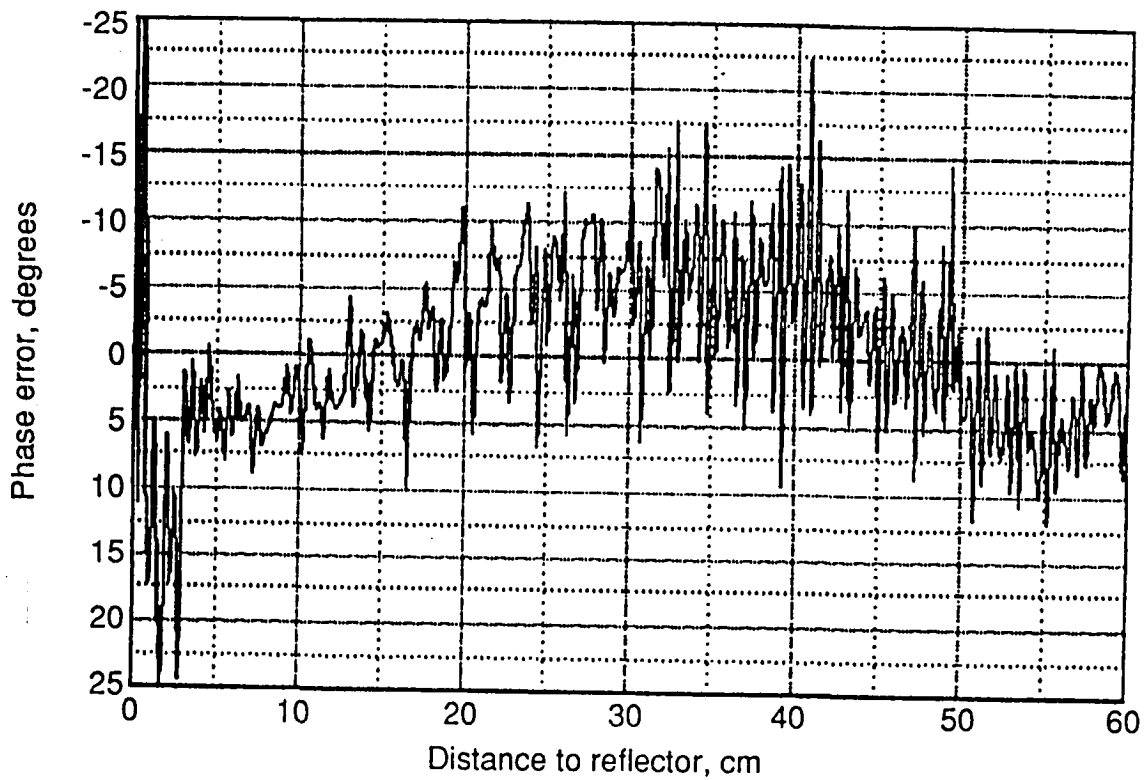


Figure 17. Measured phase error as a function of distance.

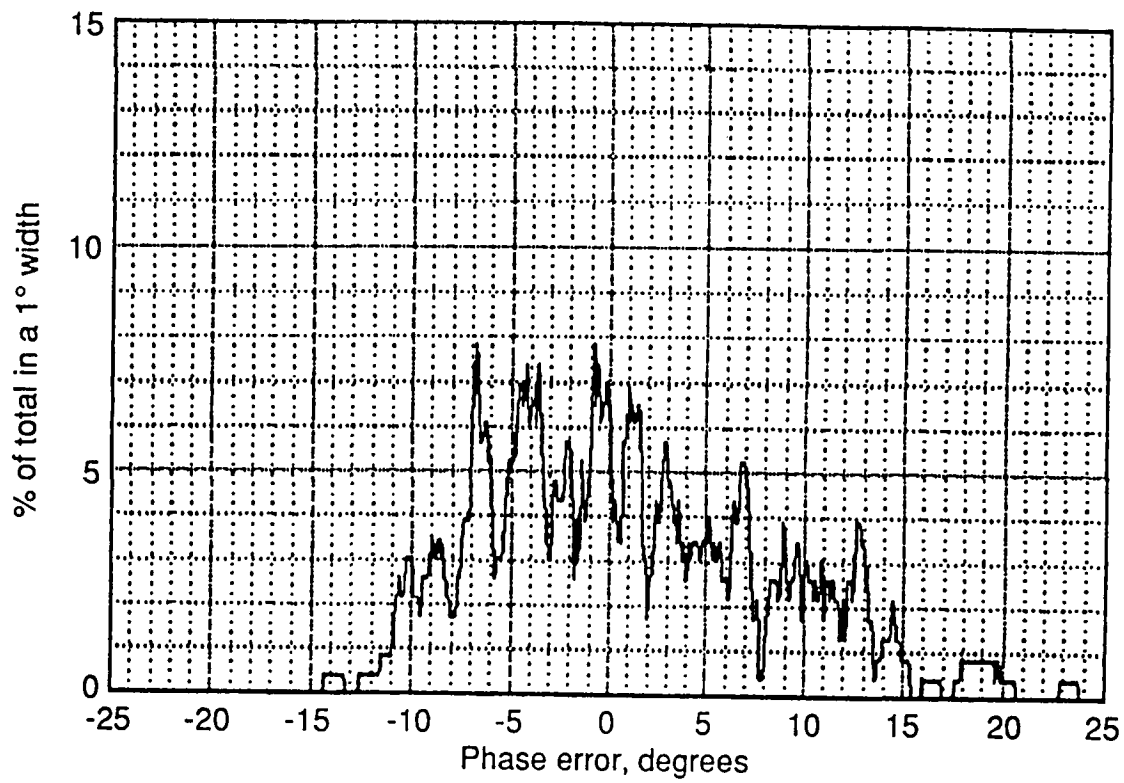
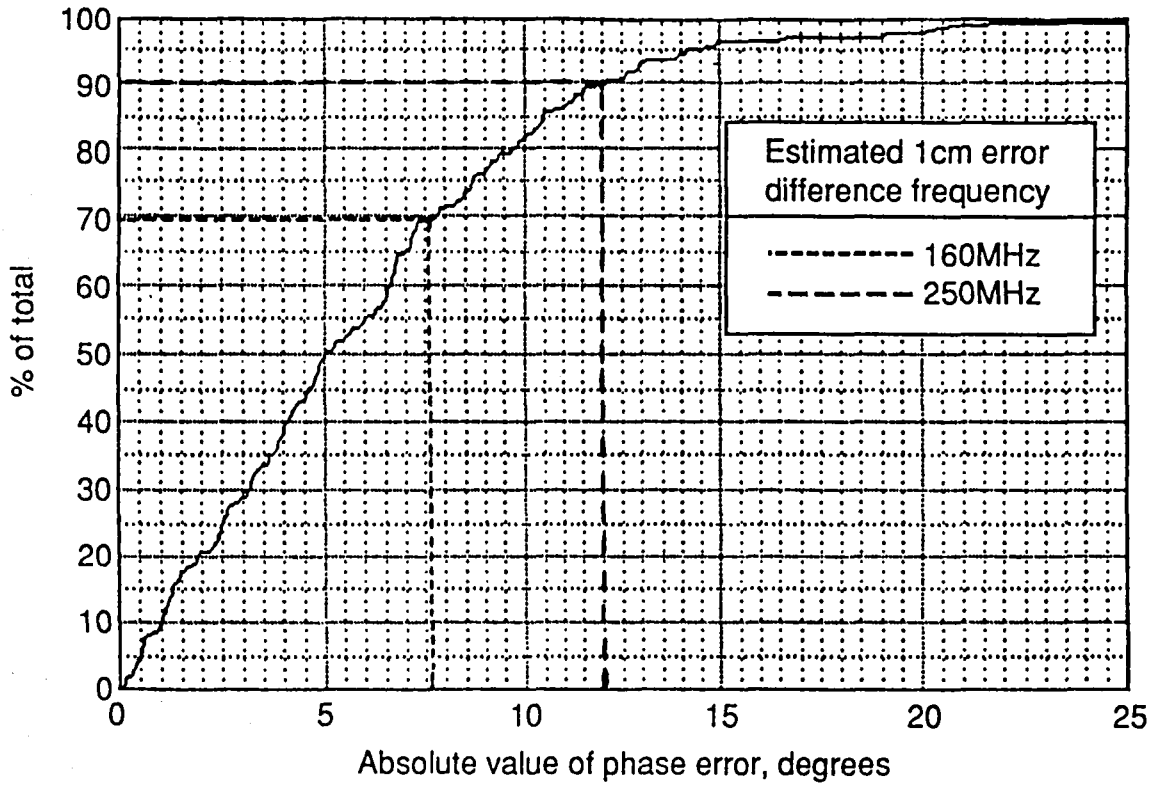


Figure 18. Measured phase error distribution (3 - 60cm).



**Test Conditions:**

Carrier freq. = 25.4GHz, AM freq. = 80MHz, Peak FM dev = 1GHz,  
 Xmit power = 3dBm, Ant. Dia. = 2.65cm, Ant. tilt = 0°, Ant. spacing = 3.15cm,  
 Ground plane = 18 x 18 inches, Reflection plane = 18 x 18 inches.

Figure 19. Cumulative distribution of measured absolute phase error (3 - 60cm).

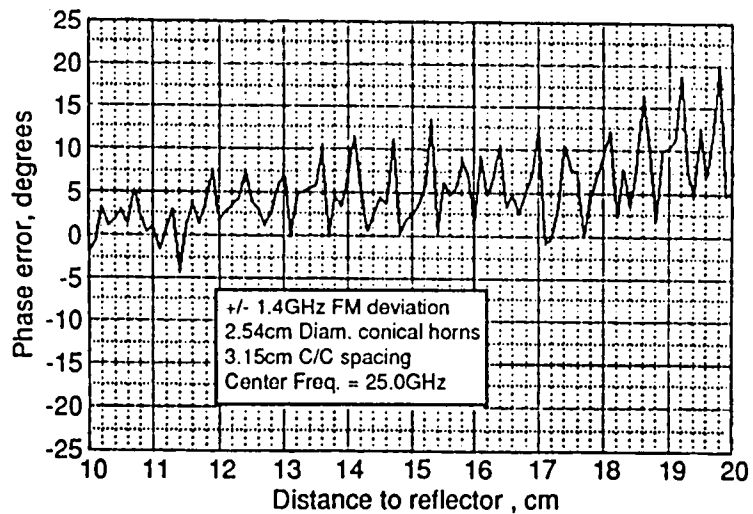
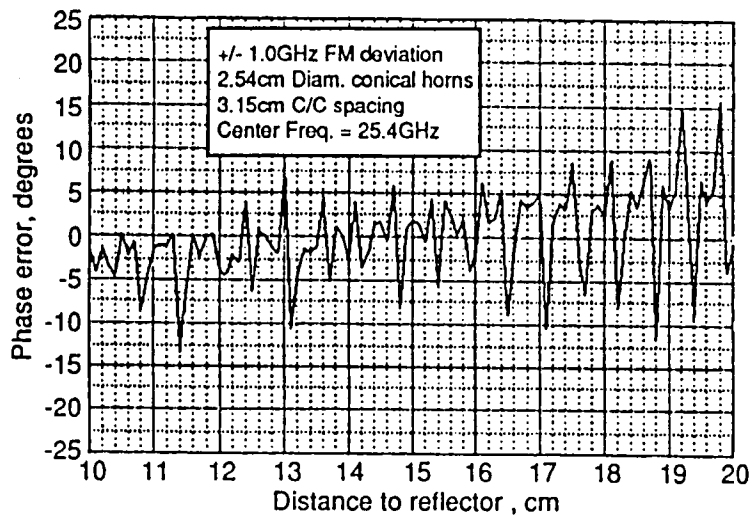
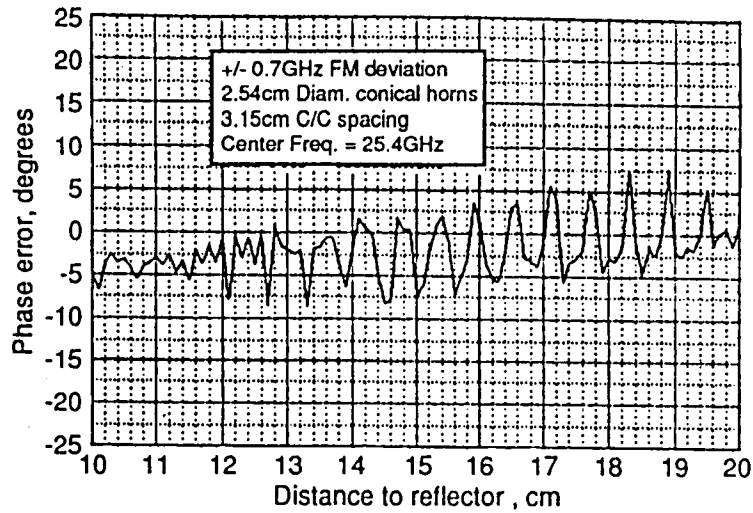


Figure 20. Experimental phase error measurements as a function of distance and FM deviation.

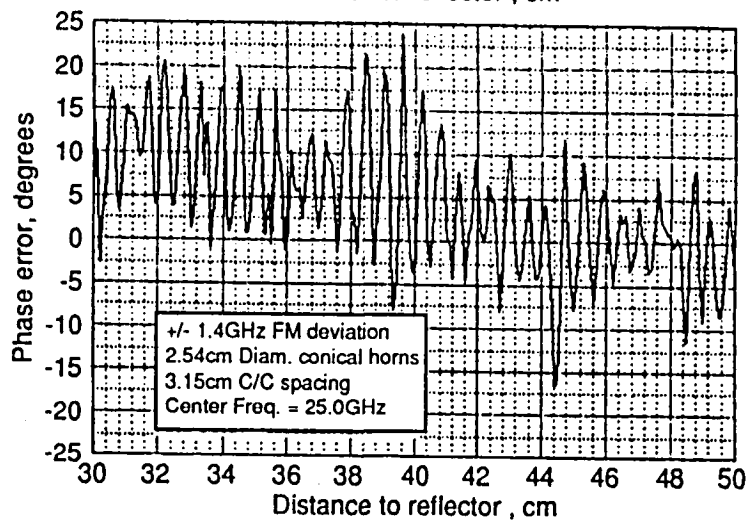
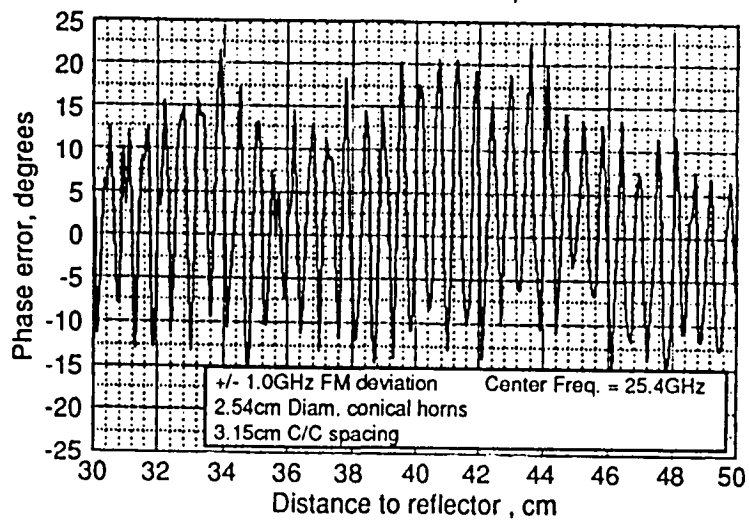
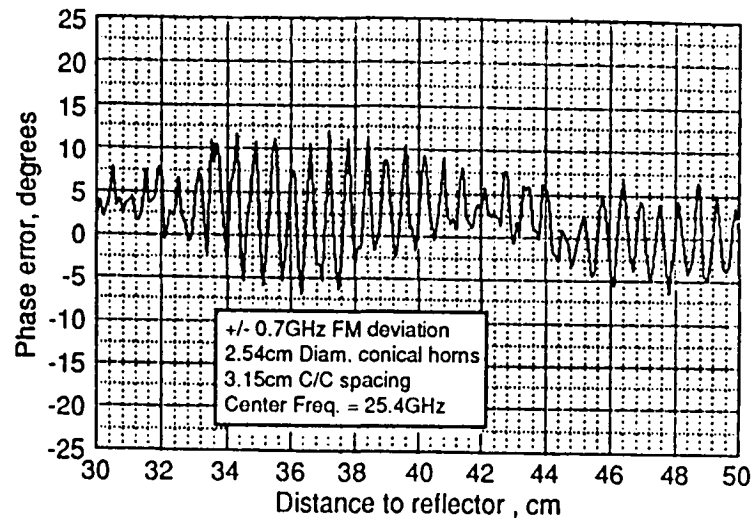
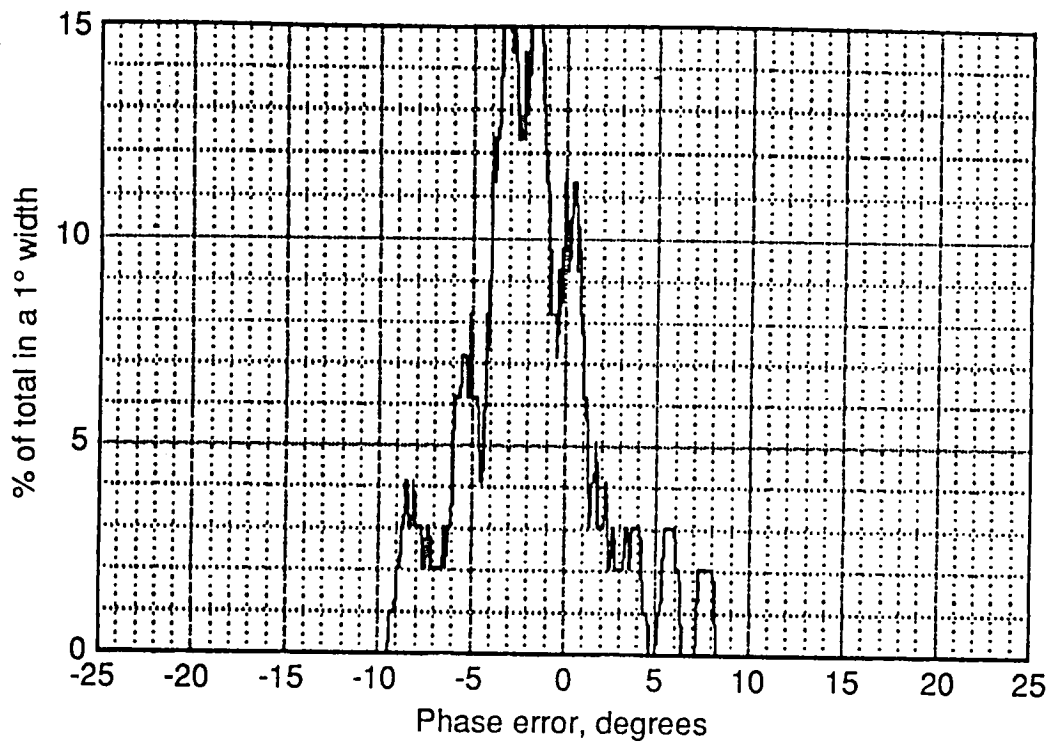
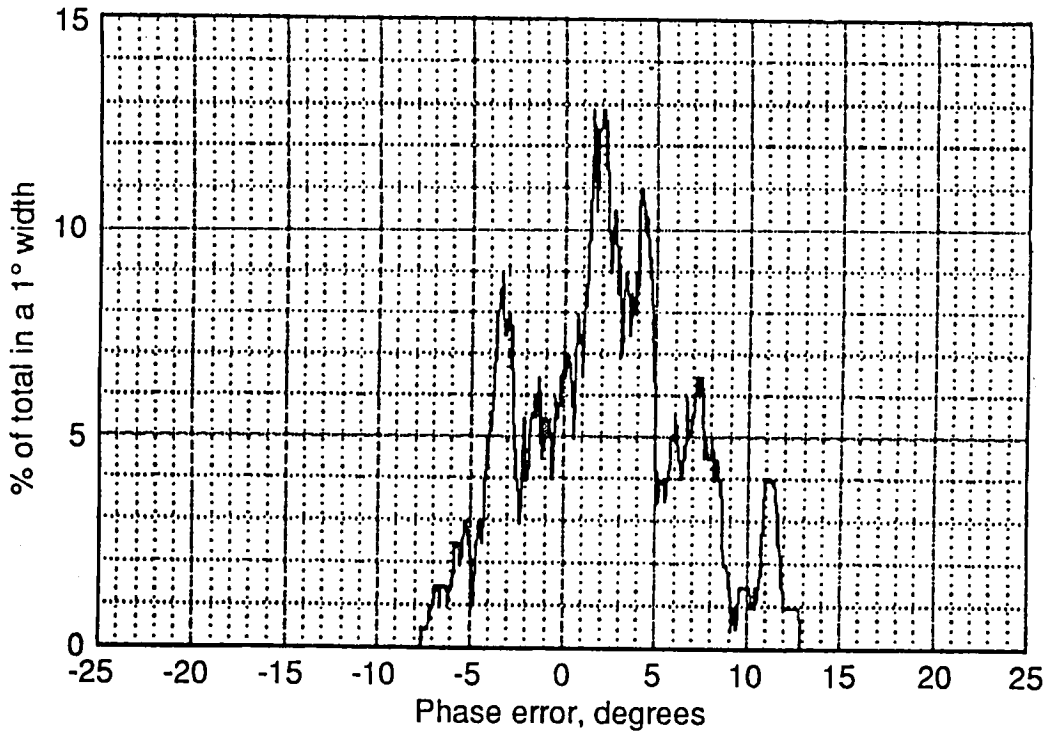


Figure 21. Experimental phase error measurements as a function of distance and FM deviation.

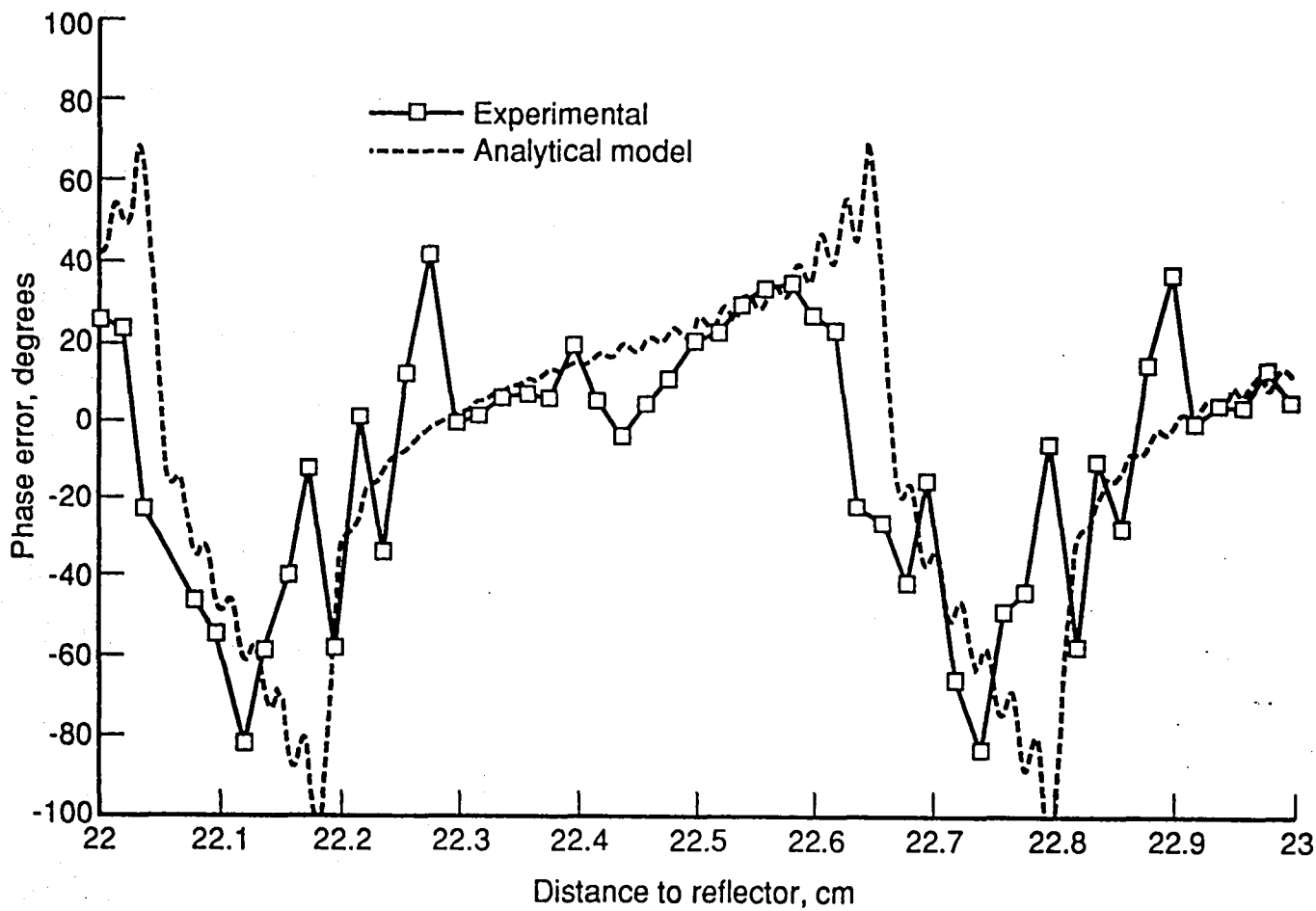


(a) Distance range of 10 - 20cm



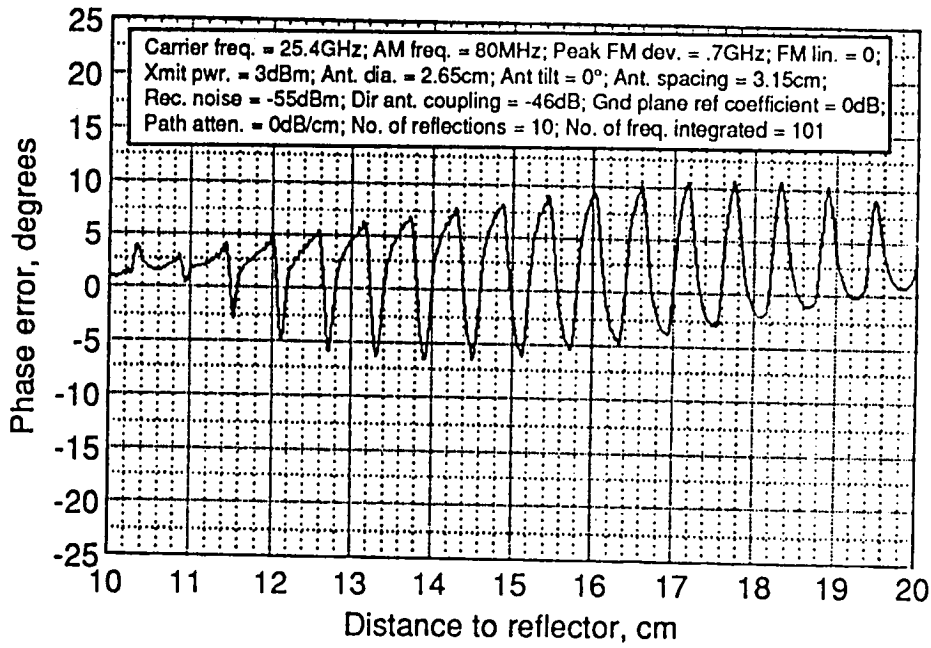
(b) Distance range of 30 - 50cm

Figure 22. Measured phase error distribution with an FM deviation of  $\pm 0.7$ GHz.

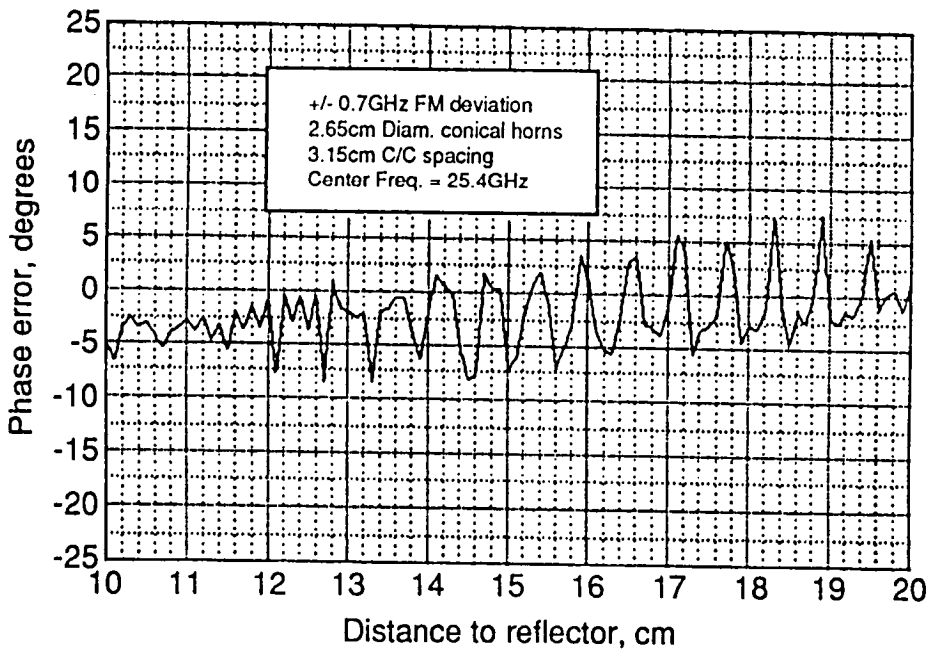


Carrier frequency: 24.4GHz  
 AM frequency: 80MHz  
 Dual antennas

Figure 23. Comparison of analytical model and experimental data illustrating multipath interference pattern.

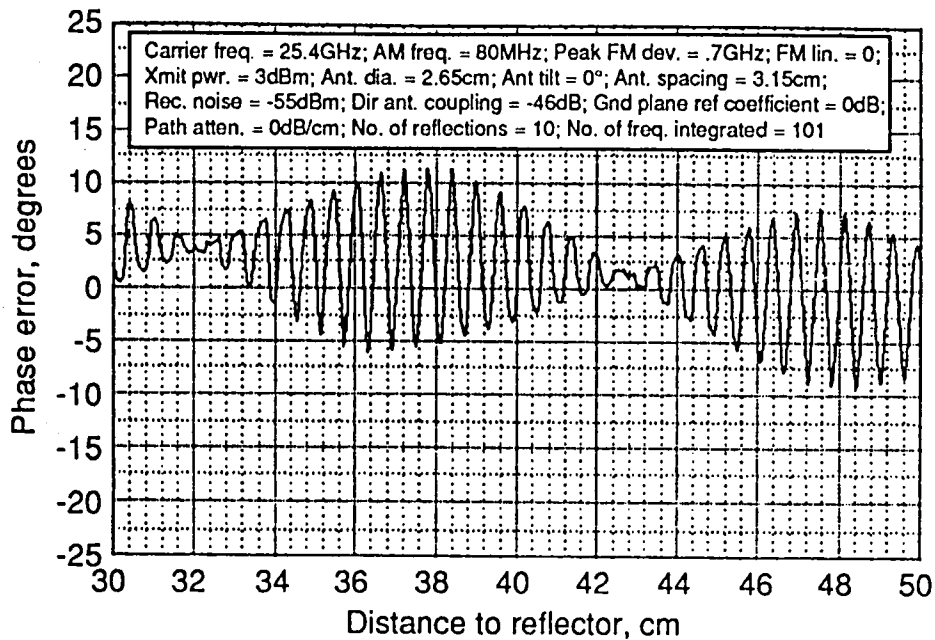


(a) Theoretical results; sine-cosine averaging

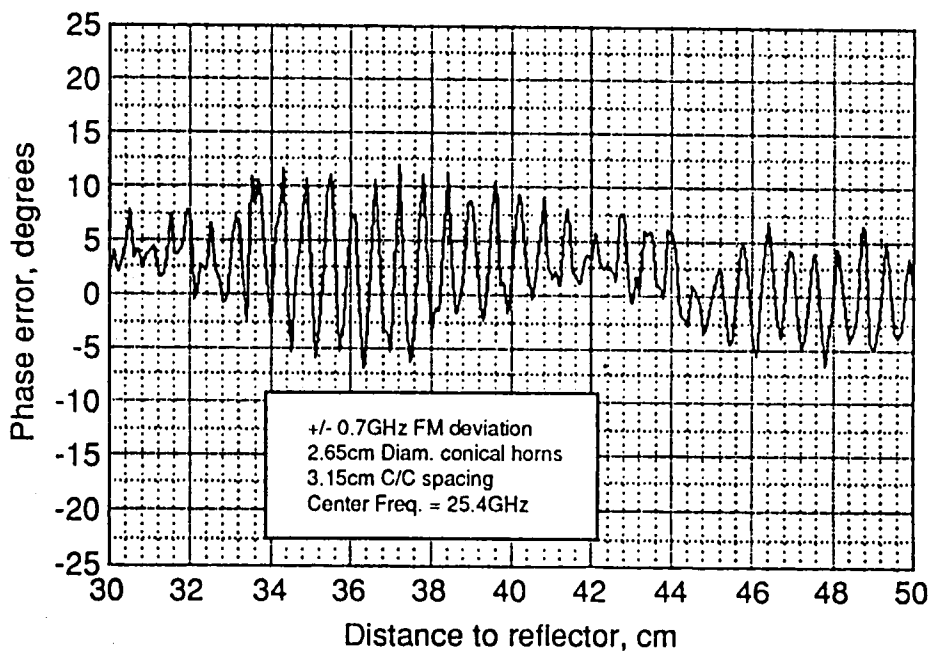


(b) Experimental results; sine-cosine averaging

Figure 24. Comparison of theoretical and experimental results of phase error with an FM deviation of  $\pm 0.7$ GHz for standoff distances from 10 - 20cm.

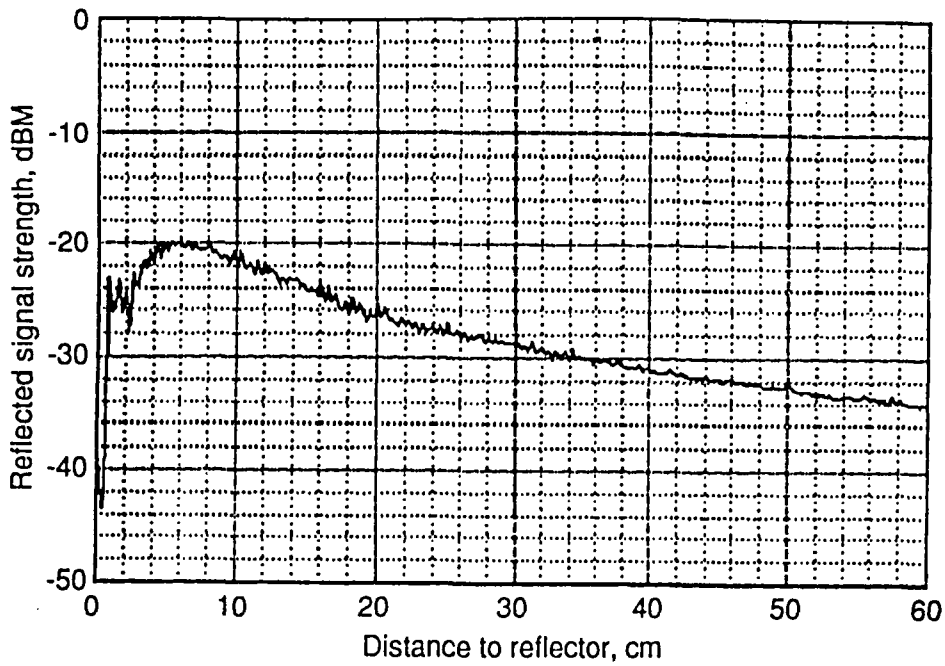


(a) Theoretical results; sine-cosine averaging



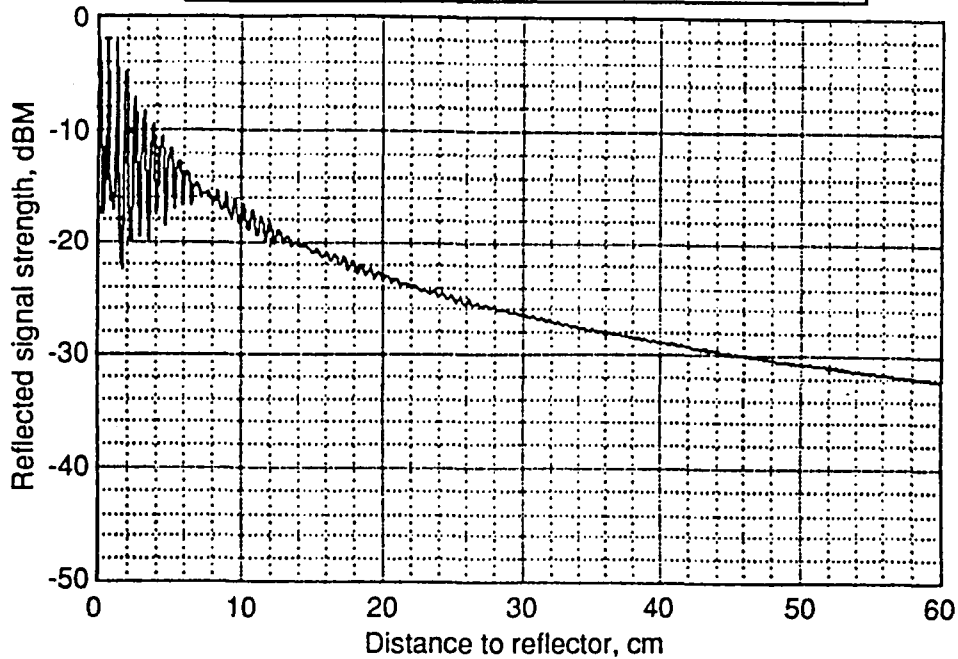
(b) Experimental results; sine-cosine averaging

Figure 25. Comparison of theoretical and experimental results of phase error with an FM deviation of  $\pm 0.7$ GHz for standoff distances from 30 - 50cm.



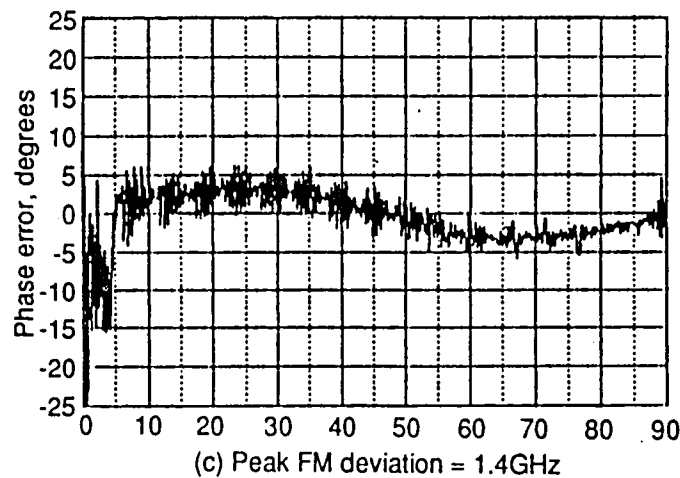
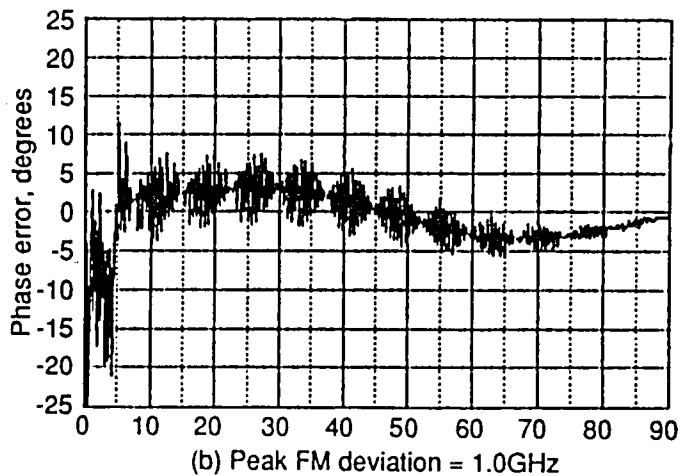
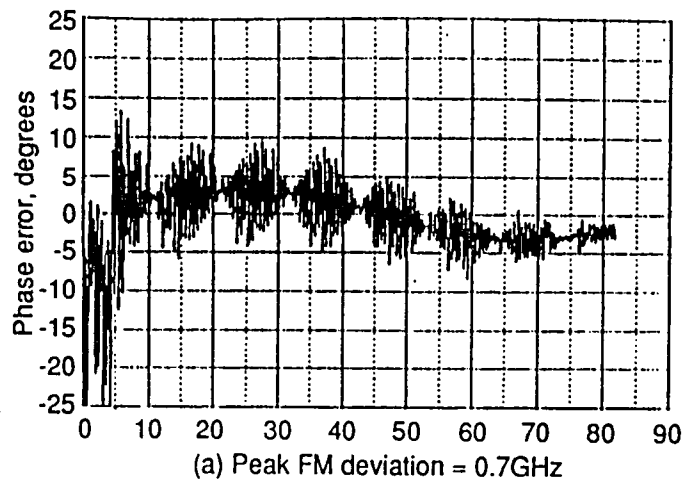
(a) Measured results

Carrier freq. = 25.4GHz; AM freq. = 80MHz; Peak FM dev. = 1GHz; FM lin. = 0;  
 Xmit pwr. = 3dBm; Ant. dia. = 1.9cm; Ant tilt = 0°; Ant. spacing = 3.15cm;  
 Rec. noise = -55dBm; Dir ant. coupling = -50dB; Gnd plane ref coefficient = 0dB;  
 Path atten. = 0dB/cm; No. of reflections = 10; No. of freq. integrated = 101



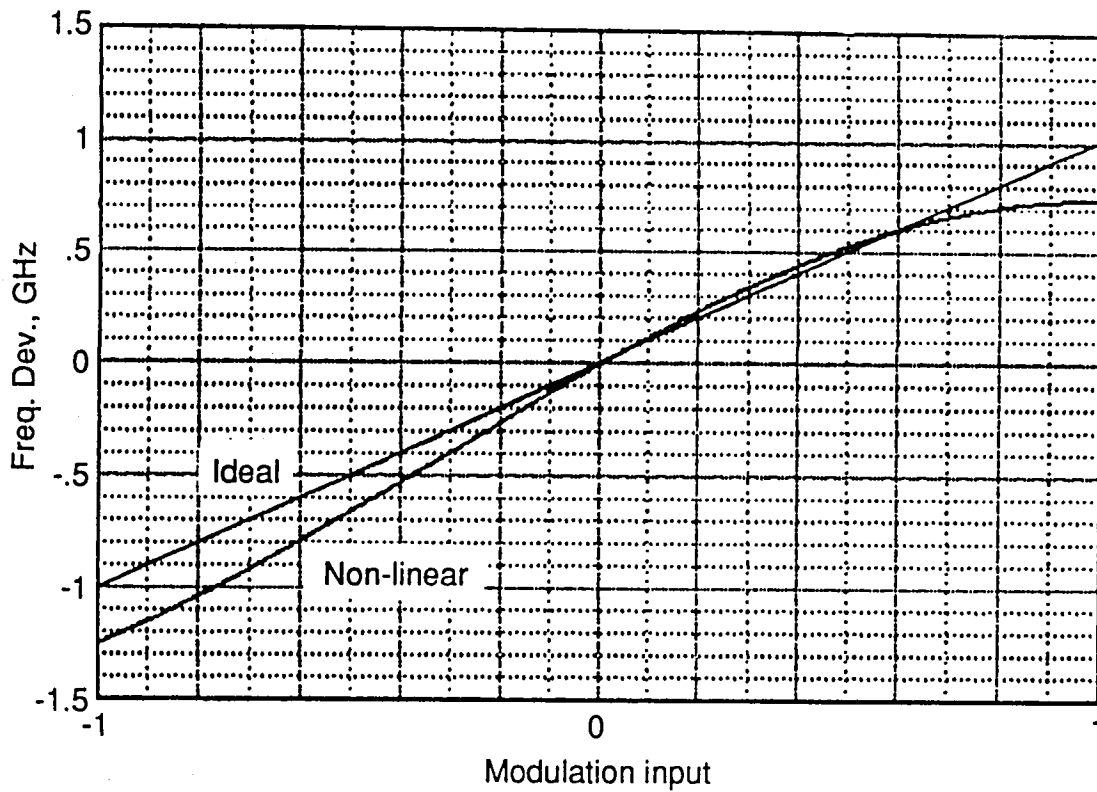
(b) Theoretical data

Figure 26. Comparison of signal strength as a function of distance for measured and theoretical data.



Carrier freq. = 25.4GHz; AM freq. = 80MHz; Peak FM dev. = as noted;  
 Xmit pwr. = 3dBm; Ant. dia. = 2.54cm; Ant tilt = 0°; Ant. spacing = 3.15cm;  
 Rec. noise = -55dBm; Dir ant. coupling = -60dB; Gnd plane ref coefficient = 0dB;  
 Path atten. = 0dB/cm; No. of reflections = 50; No. of freq. integrated = 101

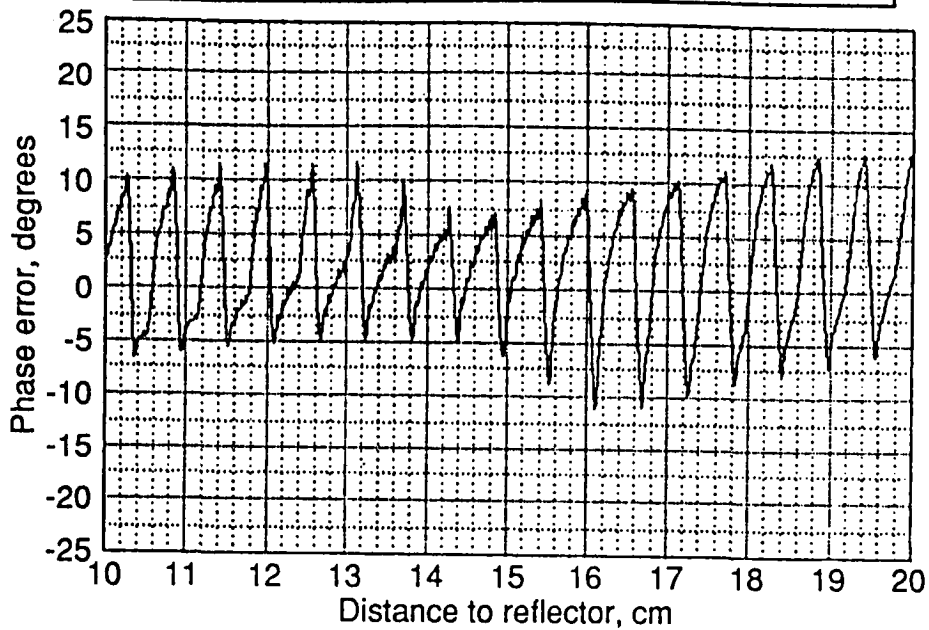
Figure 27. Comparison of computer-model data of phase error as a function of distance (0-90cm) using sine-cosine averaging with the variable peak FM deviation.



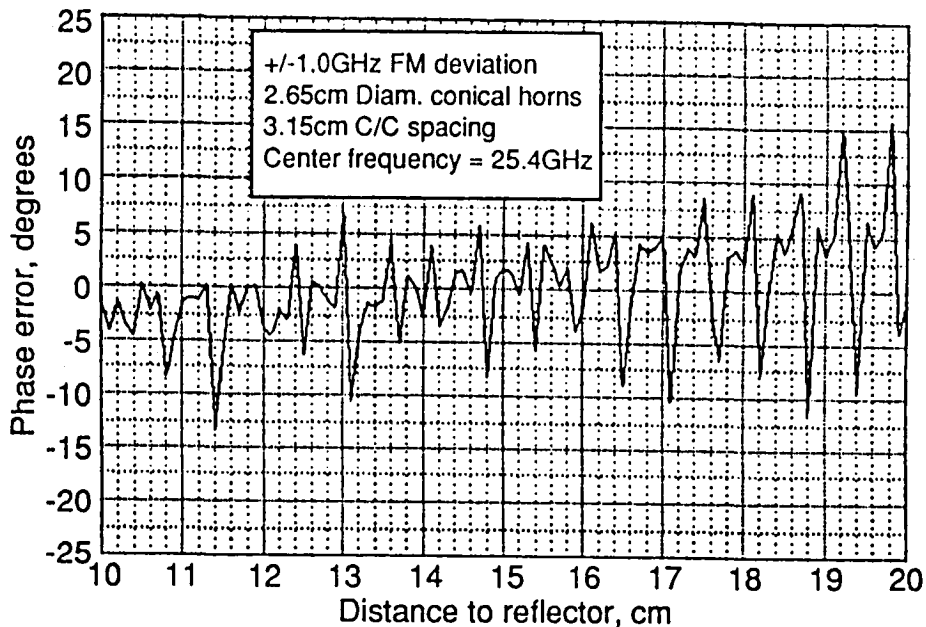
Carrier frequency = 25.4GHz  
 Peak FM deviation = 1.0GHz  
 FM non-linearity = 0.2  
 (2nd & 3rd order terms)

Figure 28. Assumed non-linear FM characteristic.

Carrier freq. = 25.4GHz; AM freq. = 80MHz; Peak FM dev. = 1GHz; FM lin. = .2;  
 Xmit pwr. = 3dBm; Ant. dia. = 2.65cm; Ant tilt = 0°; Ant. spacing = 3.15cm;  
 Rec. noise = -55dBm; Dir ant. coupling = -46dB; Gnd plane ref coefficient = 0dB;  
 Path atten. = 0dB/cm; No. of reflections = 10; No. of freq. integrated = 101



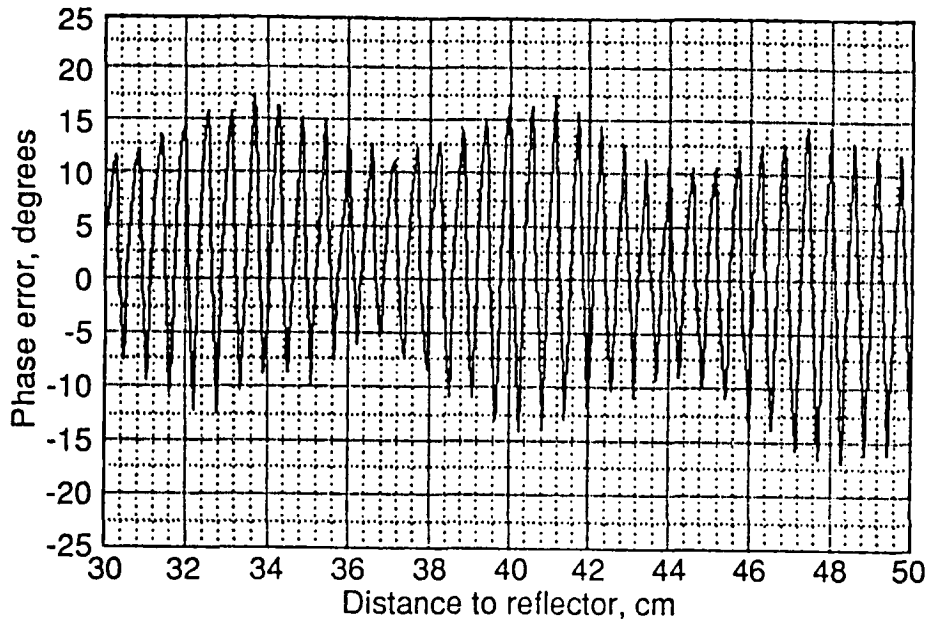
(a) Theoretical results, sine-cosine averaging



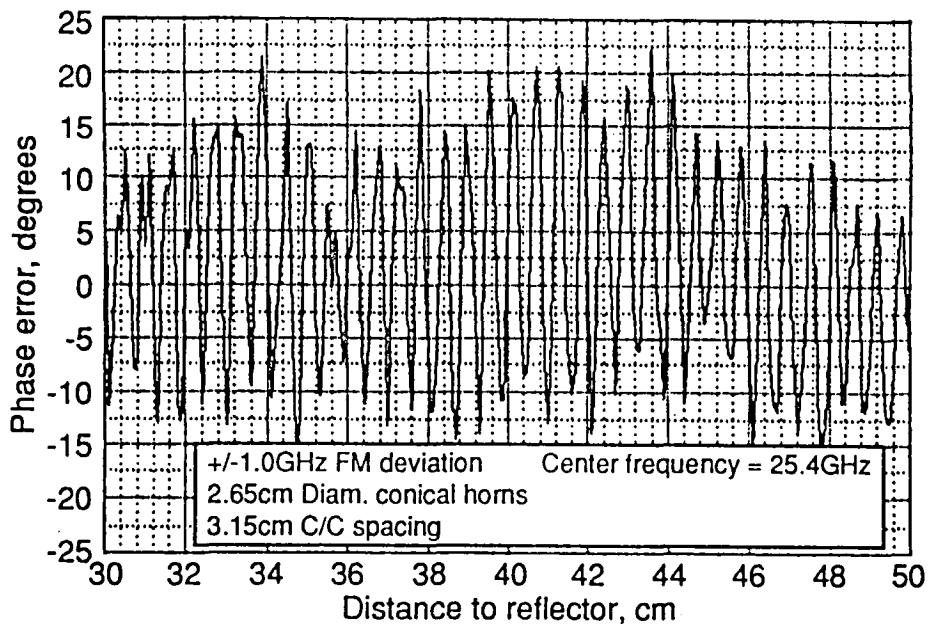
(b) Experimental results, sine-cosine averaging

Figure 29. Comparison of theoretical and experimental results of phase error with an FM deviation of  $\pm 1.0$ GHz for standoff distances from (10-20cm).

Carrier freq. = 25.4GHz; AM freq. = 80MHz; Peak FM dev. = 1GHz; FM lin. = .2;  
 Xmit pwr. = 3dBm; Ant. dia. = 2.65cm; Ant tilt = 0°; Ant. spacing = 3.15cm;  
 Rec. noise = -55dBm; Dir ant. coupling = -46dB; Gnd plane ref coefficient = 0dB;  
 Path atten. = 0dB/cm; No. of reflections = 50; No. of freq. integrated = 101

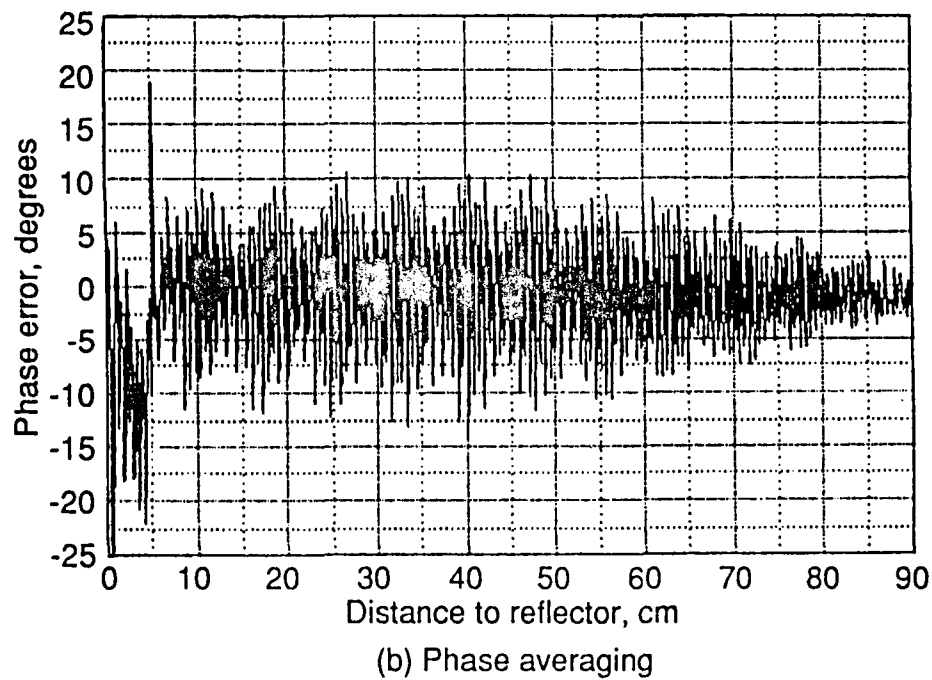
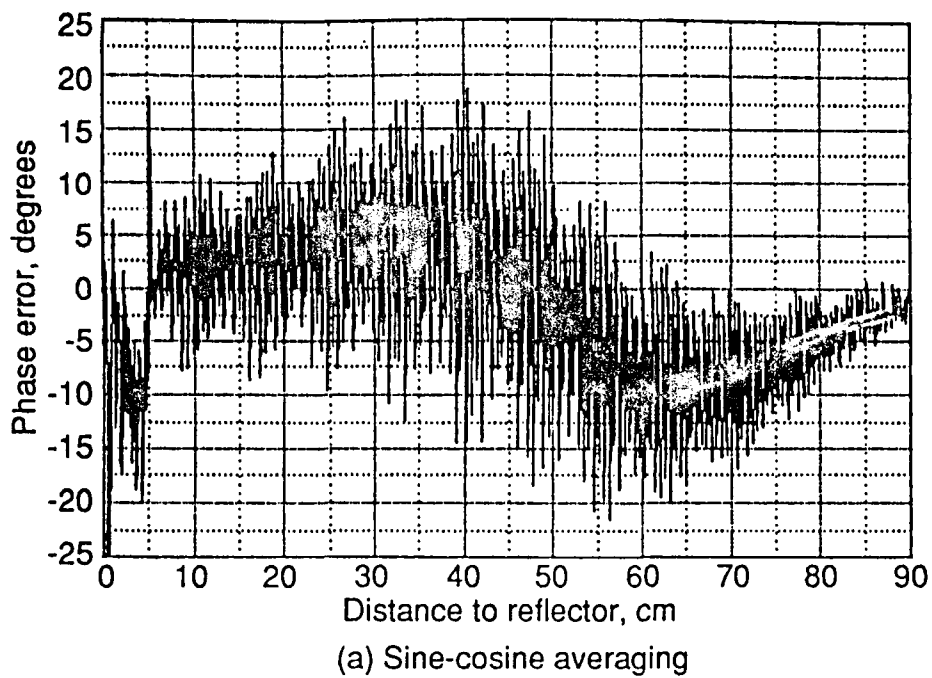


(a) Theoretical results, sine-cosine averaging



(b) Experimental results, sine-cosine averaging

Figure 30. Comparison of theoretical and experimental results of phase error with an FM deviation of  $\pm 1.0$ GHz for standoff distances from (30-50cm).



Theoretical Model Input Parameters:  
 Carrier freq. = 25.4GHz; AM freq. = 80MHz; Peak FM dev. = 1GHz; FM lin. = .2;  
 Xmit pwr. = 3dBm; Ant. dia. = 2.54cm; Ant tilt = 0°; Ant. spacing = 3.15cm;  
 Rec. noise = -55dBm; Dir ant. coupling = -44dB; Gnd plane ref coefficient = 0dB;  
 Path atten. = 0dB/cm; No. of reflections = 50; No. of freq. integrated = 101

Figure 31. Theoretical comparison of resultant phase error for sine-cosine averaging and phase averaging.

Carrier freq. = 25GHz; AM freq. = 125MHz; Peak FM dev. = 1GHz; FM lin. = .1;  
Xmit pwr. = 3dBm; Ant. dia. = 2.65cm; Ant tilt = 0°; Ant. spacing = 3.15cm;  
Rec. noise = -55dBm; Dir ant. coupling = -50dB; Gnd plane ref coefficient = 0dB;  
Path atten. = .25dB/cm; No. of reflections = 10; No. of freq. integrated = 41

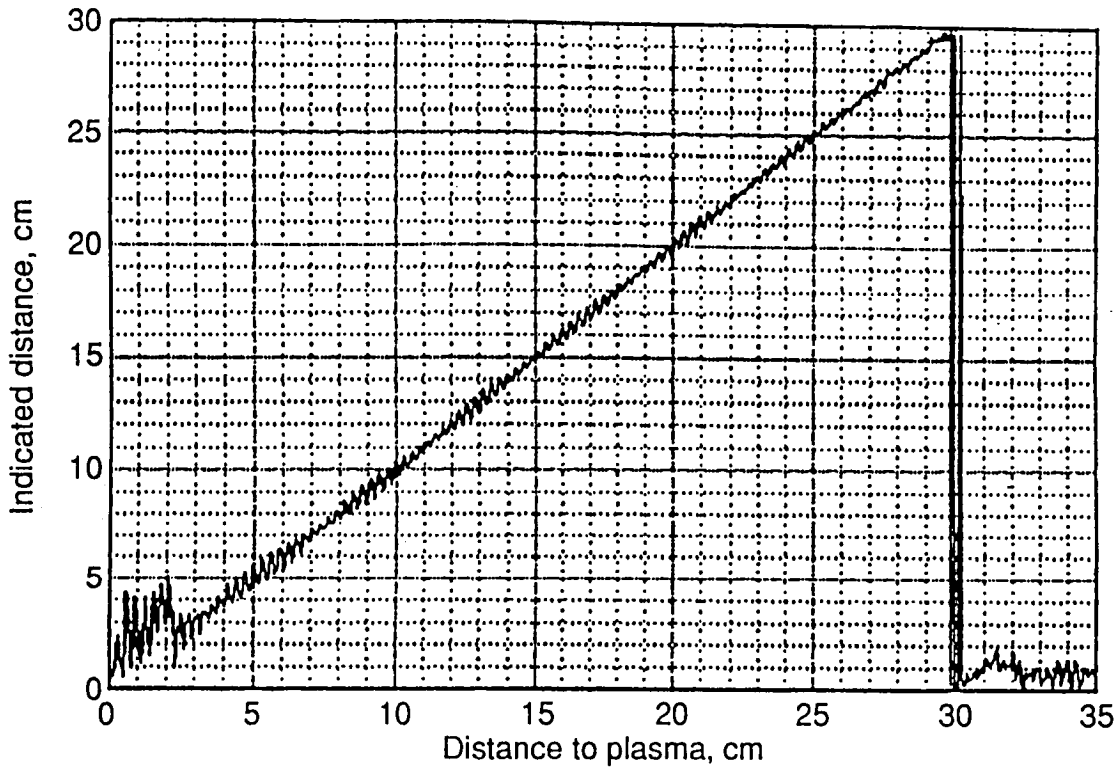


Figure 32. Theoretical model results, using phase averaging, of indicated distance from plasma reflection boundary.

Carrier freq. = 25GHz; AM freq. = 125MHz; Peak FM dev. = 1GHz; FM lin. = .1;  
Xmit pwr. = 3dBm; Ant. dia. = 2.65cm; Ant tilt = 0°; Ant. spacing = 3.15cm;  
Rec. noise = -55dBm; Dir ant. coupling = -50dB; Gnd plane ref coefficient = 0dB;  
Path atten. = .25dB/cm; No. of reflections = 10; No. of freq. integrated = 41

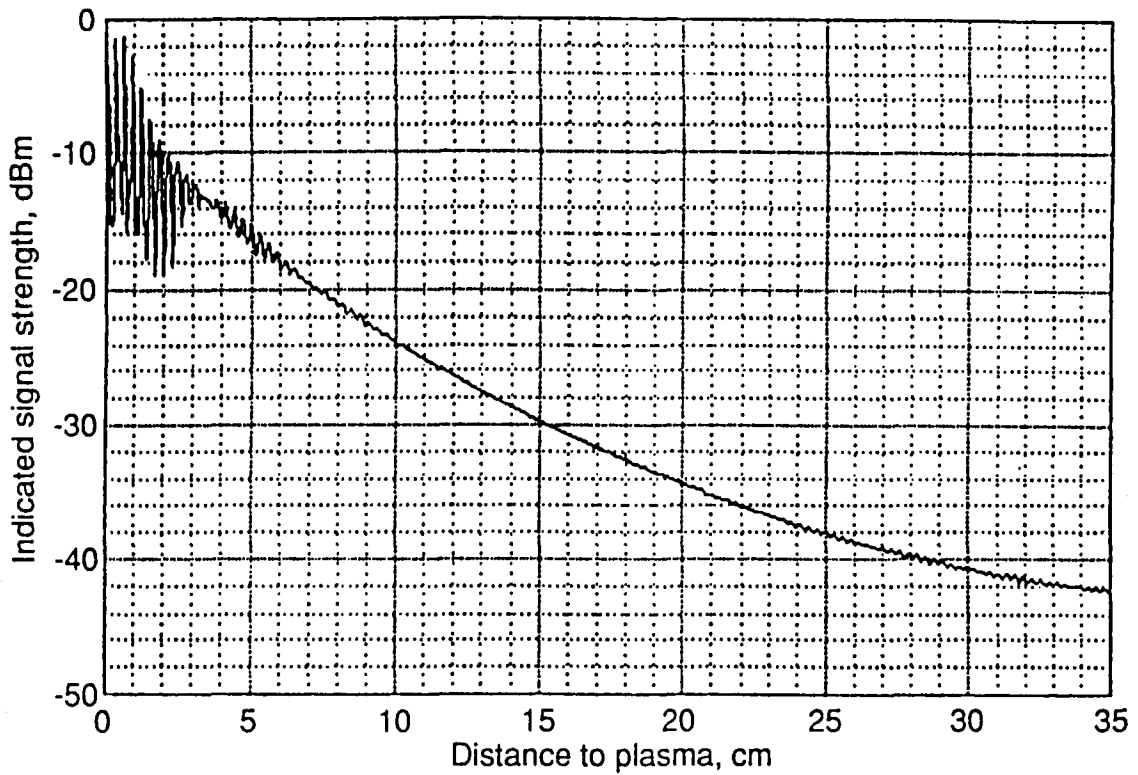
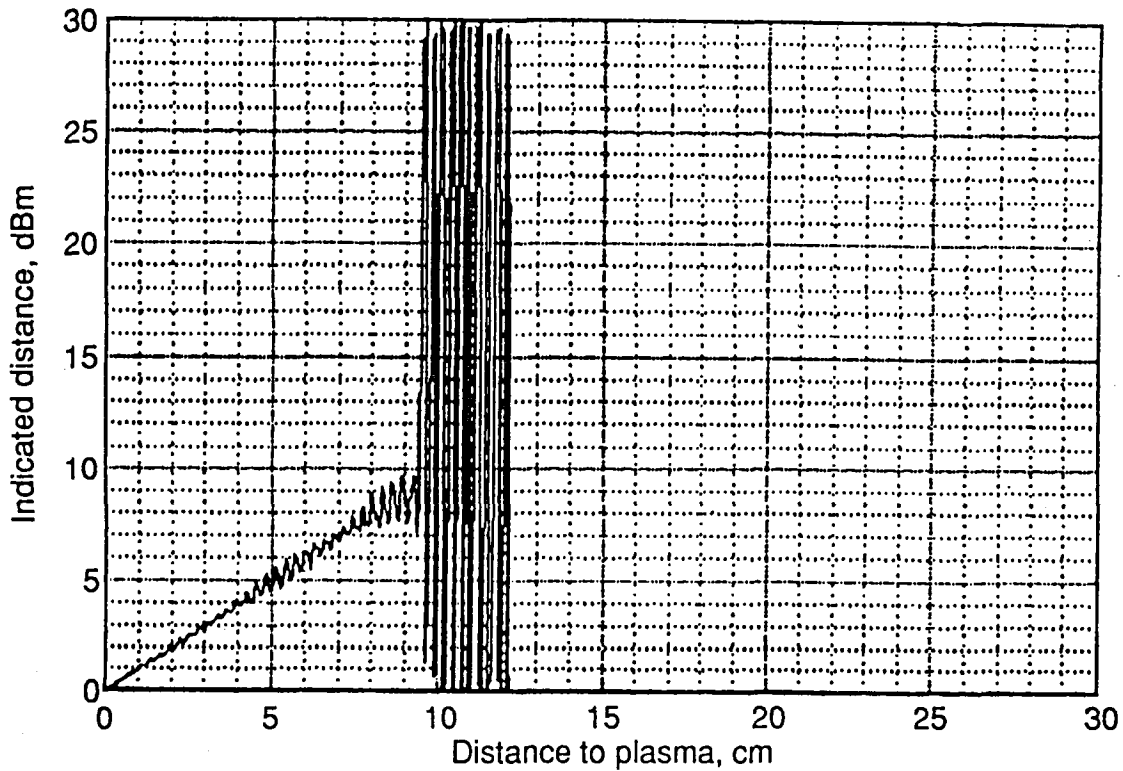


Figure 33. Theoretical-model results of indicated signal strength from a reflecting plasma.

Carrier freq. = 25GHz; AM freq. = 125MHz; Peak FM dev. = 1GHz; FM lin. = .1;  
Xmit pwr. = 3dBm; Ant. dia. = 2.65cm; Ant tilt = 0°; Ant. spacing = 0cm;  
Rec. noise = -55dBm; Dir ant. coupling = -30dB; Gnd plane ref coefficient = 0dB;  
Path atten. = .25dB/cm; No. of reflections = 10; No. of freq. integrated = 21



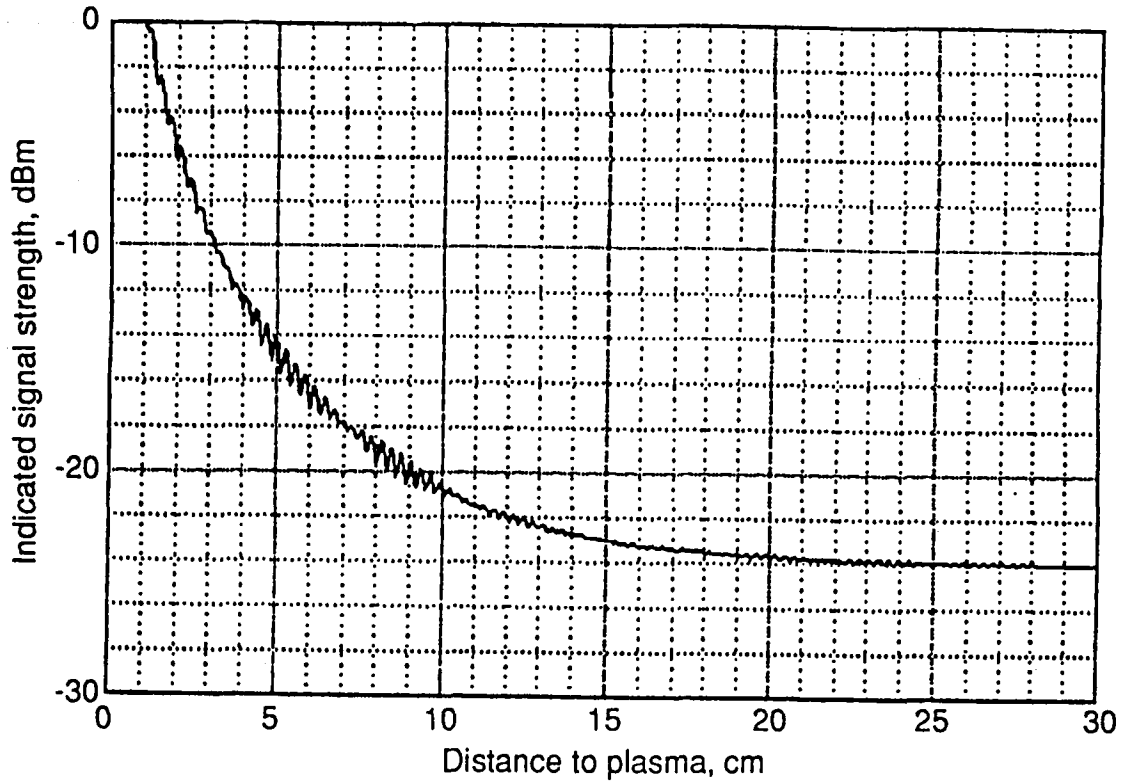
Monostatic system:

Transmit aperture only,

Signal leakage from transmit into receive line = -30dB

Figure 34. Theoretical-model results, using phase averaging, of indicated distance from a plasma reflection boundary.

Carrier freq. = 25GHz; AM freq. = 125MHz; Peak FM dev. = 1GHz; FM lin. = .1;  
Xmit pwr. = 3dBm; Ant. dia. = 2.65cm; Ant tilt = 0°; Ant. spacing = 0cm;  
Rec. noise = -55dBm; Dir ant. coupling = -30dB; Gnd plane ref coefficient = 0dB;  
Path atten. = .25dB/cm; No. of reflections = 10; No. of freq. integrated = 21

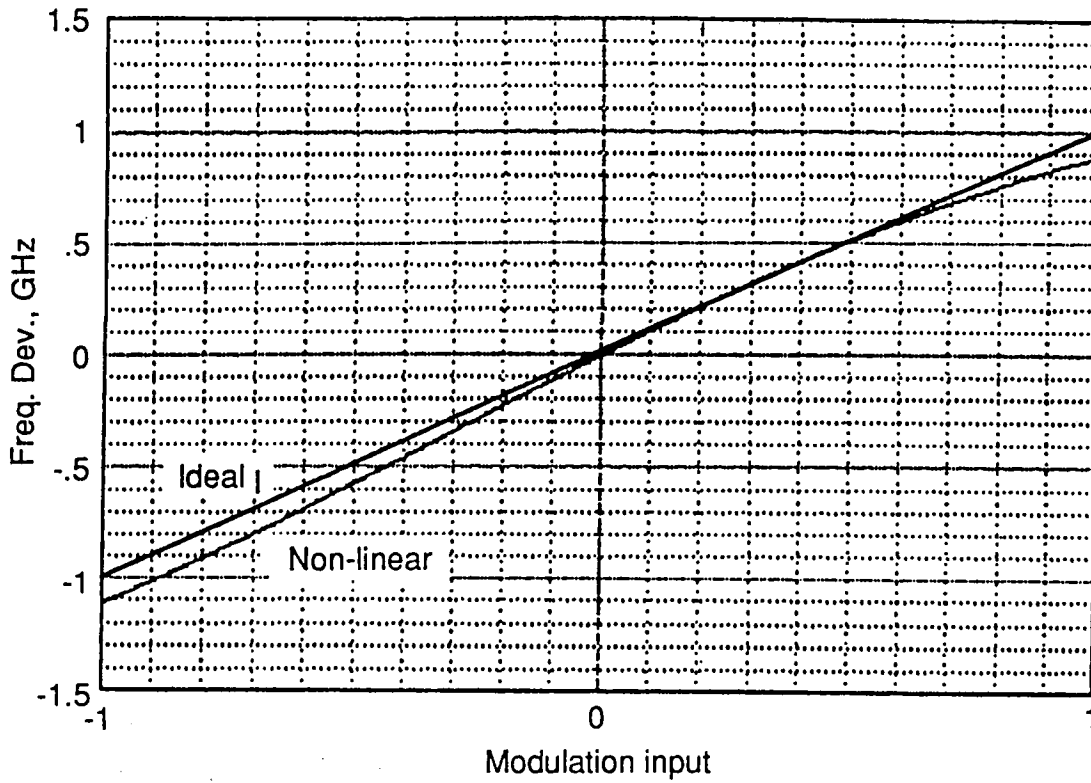


Monostatic system:

Transmit aperture only,

Signal leakage from transmit into receive line = -30dB

Figure 35. Theoretical-model results of indicated received signal strength from a reflecting plasma.



Carrier frequency = 25GHz  
 Peak FM deviation = 1.0GHz  
 FM non-linearity = 0.1  
 (2nd & 3rd order terms)

Figure 36. Non-linear FM characteristics.



# REPORT DOCUMENTATION PAGE

*Form Approved*  
OMB No. 0704-0188

Public reporting burden for this collection of information is estimated to average 1 hour per response, including the time for reviewing instructions, searching existing data sources, gathering and maintaining the data needed, and completing and reviewing the collection of information. Send comments regarding this burden estimate or any other aspect of this collection of information, including suggestions for reducing this burden, to Washington Headquarters Services, Directorate for Information Operations and Reports, 1215 Jefferson Davis Highway, Suite 1204, Arlington, VA 22202-4302, and to the Office of Management and Budget, Paperwork Reduction Project (0704-0188), Washington, DC 20503.

<b>1. AGENCY USE ONLY (Leave blank)</b>		<b>2. REPORT DATE</b> June 1993	<b>3. REPORT TYPE AND DATES COVERED</b> Technical Memorandum	
<b>4. TITLE AND SUBTITLE</b> The MRIS Feasibility Study			<b>5. FUNDING NUMBERS</b> WU 505-64-12-04	
<b>6. AUTHOR(S)</b> Robert T. Neece, Aubrey E. Cross, and James H. Schrader				
<b>7. PERFORMING ORGANIZATION NAME(S) AND ADDRESS(ES)</b> NASA Langley Research Center Hampton, VA 23681-0001			<b>8. PERFORMING ORGANIZATION REPORT NUMBER</b>	
<b>9. SPONSORING/MONITORING AGENCY NAME(S) AND ADDRESS(ES)</b> National Aeronautics and Space Administration Washington, DC 20546-0001			<b>10. SPONSORING/MONITORING AGENCY REPORT NUMBER</b> NASA TM-107763	
<b>11. SUPPLEMENTARY NOTES</b> Neece: Langley Research Center, Hampton, VA; Cross: Research Triangle Institute, Hampton, VA; Schrader: Research Triangle Institute, Hampton, VA				
<b>12a. DISTRIBUTION / AVAILABILITY STATEMENT</b> Unclassified-Unlimited  Subject Category 32			<b>12b. DISTRIBUTION CODE</b>	
<b>13. ABSTRACT (Maximum 200 words)</b>  The Microwave Reflectometer Ionization Sensor (MRIS) is an instrument being developed for use in detecting and ranging of electron density layers in the reentry plasma of a space transfer vehicle. This paper presents the rationale for the selection of the Double Sideband Suppressed Carrier (DSBSC) system used in the feasibility study for the MRIS. A 25 GHz single-oscillator system and a 220 GHz double-oscillator system are described. The 25 GHz system was constructed and tested in the laboratory and test results are presented. As developed, the system employs a sideband spacing of 160 MHz. Based on an estimated electromagnetic wave velocity in the plasma, a round-trip phase shift measurement accuracy of $\pm 7.6^\circ$ was required for the desired $\pm 1/2$ cm distance measurement accuracy. The interaction of parallel ground and reflecting planes produces interference that prevents the basic DSBSC system from meeting the accuracy goal, so a frequency modulation was added to the system to allow averaging of the measured phase deviation. With an FM deviation of $\pm 1$ GHz, laboratory measurements were made for distances from 5 to 61 cm in free space. Accounting for the plasma velocity factor, 82 percent of the data were equal to or better than the desired accuracy. Based on this measured result, a sideband spacing to 250 MHz could be expected to yield data approximately 96 percent within the accuracy goal.				
<b>14. SUBJECT TERMS</b> Aeroassist Flight Experiment (AFE), Microwave Reflectometer Ionization Sensor (MRIS), reflectometer, radar, plasma, aerobrake			<b>15. NUMBER OF PAGES</b> 74	
			<b>16. PRICE CODE</b> A04	
<b>17. SECURITY CLASSIFICATION OF REPORT</b> Unclassified	<b>18. SECURITY CLASSIFICATION OF THIS PAGE</b> Unclassified	<b>19. SECURITY CLASSIFICATION OF ABSTRACT</b>	<b>20. LIMITATION OF ABSTRACT</b>	

4

3

•

3

